ISSN 0023-1584, Kinetics and Catalysis, 2010, Vol. 51, No. 2, pp. 162–193. © Pleiades Publishing, Ltd., 2010.
Original Russian Text © V.I. Anikeev, A. Ermakova, A.M. Chibiryaev, I.V. Kozhevnikov, 2010, published in Kinetika i Kataliz, 2010, Vol. 51, No. 2, pp. 176–209.

Kinetics of Thermal Conversions of Monoterpenic Compounds in Supercritical Lower Alcohols

V. I. Anikeev[a], A. Ermakova[a], A. M. Chibiryaev[b], and I. V. Kozhevnikov[a]

[a] *Boreskov Institute of Catalysis, Siberian Branch, Russian Academy of Sciences, Novosibirsk, 630090 Russia*

[b] *Novosibirsk Institute of Organic Chemistry, Siberian Branch, Russian Academy of Sciences, Novosibirsk, 630090 Russia*

e-mail: anik@catalysis.nsk.su

Received January 16, 2009

Abstract—The most important information concerning thermal conversions of vegetable terpenes (α-pinene, β-pinene, turpentine, and *cis*-verbenol) in supercritical lower alcohols is systematized. The kinetics of selected reactions is reported and is compared with the kinetics of the same reactions in the gas and liquid phases. Thermodynamic calculations of the phase states and kinetic parameters are presented for a number of multicomponent multiphase systems containing terpenes and lower alcohols. The effect of the supercritical solvent pressure on the rate and selectivity of the selected reactions is reported.

DOI: 10.1134/S0023158410020035

INTRODUCTION

Heat-induced chemical conversions of (mono)terpenic compounds of vegetable origin are of considerable practical interest for they are used in the synthesis of C_7–C_{10} alkylated benzenes, various monooxygenated and polyoxygenated compounds for medicinal applications (active components of pharmaceuticals, aromatherapy), diene and triene compounds (semiproducts for fine organic synthesis), and monomers to be polymerized or oligomerized. For example, the noncatalytic thermolysis of the bicyclic monoterpenic hydrocarbons α- and β-pinene, which are the main components of turpentine, yields limonene and β-myrcene, which are used in the production of cosmetics, perfumery, and household chemicals.

α-Pinene is among the most abundant monoterpenic hydrocarbons in nature [1]. Its industrial sources are various kinds of turpentine from softwood. Biosynthesis in plants produces both α-pinene enantiomers, one of them being usually dominant. Pinene is a convenient starting chemical for producing fragrance compounds and perfume compositions [2–5] and a valuable semiproduct for the pharmaceutical industry [2, 5]. For example, the thermal isomerization of α-pinene in the gas phase [6–19] or in the liquid phase [11, 12, 15, 16, 20–25] yields mixture of monocyclic and acyclic compounds, such as limonene, alloocimene and pyronene isomers, and substituted cyclohexenes. This mixture is typically dominated by the monocyclic C_{10} diene limonene.

β-Pinene is a monoterpenic bicyclic hydrocarbon present in turpentines and the essential oils of plants. The turpentine of some coniferous trees contains up to 90% β-pinene. Biosynthesis in plants produces both β-pinene enatiomers. As a rule, one of them is much more abundant. β-Pinene is the starting chemical for the synthesis of β-myrcene, an important component of natural and synthetic perfume compositions [18, 19, 26] and a convenient synthetic precursor of more valuable fragrance compounds and some carotenoids.

Verbenol is a bicyclic C_{10} terpenoid belonging to the family of monohydroxy derivatives of α-pinene. Verbenol has *cis* and *trans* isomers, and either can exist as two enantiomers, all having the pleasant odor of camphor. In nature, the verbenol isomers are the main components of the aggregation pheromones of bark beetles (*Ips* sp. and *Dendroctonus* sp.) and occur in the essential oils of some plants. At the same time they can be synthesized by the catalytic allylic oxidation of α-pinene. They are employed in the preparation of artificial perfume compositions and in the synthesis of other compounds in demand, such as citral, piperitenol isomers, and vitamin A.

Purified sulfate turpentine is obtained by processing crude turpentine, which is a by-product of sulfate cellulose production. It is a volatile monoterpene mixture consisting of α-pinene, β-pinene, Δ^3-carene, camphene, tricyclene, β-myrcene, α-terpinene, terpinolene, β-phellandrene, and a number of other compounds. In addition, sulfate turpentine contains sulfur-containing compounds (up to 0.05% sulfur). These compounds markedly limit the area of its application because they have unsuitable organoleptic properties and poison the catalysts used in its processing. Nevertheless, since sulfate turpentine contains a large proportion of α-pinene (up to 80%) and other

unsaturated hydrocarbons with bridged cyclic structures, it is viewed as a convenient and cheap raw material for obtaining a variety of valuable products [27–34]. It is largely used as a solvent for varnishes and oil paints and is a valuable starting chemical for producing synthetic camphor, a compound possessing a variety of pharmaceutical properties.

Turpentine oil is obtained by processing pine oleoresin. It is a transparent volatile liquid with a specific odor, containing no precipitate or water. The total α- and β-pinene content of turpentine oil is at least 60%. Turpentine oil is used as a raw material in organic synthesis and as a solvent. It is the starting chemical in the synthesis of camphor, a substance having manifold medicinal properties.

The chemical conversions of the above monoterpenic compounds are very diverse and have been carefully investigated. In particular, the thermal isomerization of α- and β-pinenes has been studied in detail. This reaction is usually carried out at a reduced or atmospheric pressure in the gas or liquid phase. The gas-phase thermal isomerization of α-pinene is conducted at 220–450°C [13–15, 18, 19], and the liquid-phase process is performed at 180–257°C and the corresponding saturation pressures [16, 23]. The reaction mixture residence time necessary for 90–95% α-pinene conversion may be as along as tens of hours. This long residence time hampers wide commercialization of terpene isomerization technologies both in the synthesis of polyunsaturated aliphatic compounds and in the production of the most important arenes.

The thermal isomerization rate of terpene compounds can be increased by using a catalyst [35] or a new, more favorable reaction medium. Supercritical solvents seem to be the most promising for this purpose. Supercritical fluids have already been recognized as attractive media for some organic reactions, ensuring a multifold increase in the reaction arte and selectivity control [36–38].

Among the supercritical solvents suitable for chemical reactions, water, CO_2, alcohols, and some lower saturated and unsaturated hydrocarbons have received greatest attention. In some cases, preference is given to supercritical water (SCW) and CO_2. At the same time, lower alcohols are conventional solvents for organic reactions, including those conducted under supercritical conditions. Owing to their high solvating power, in combination with comparatively small values of critical parameters (for ethanol, the critical temperature is $T_{cr} = 516.2$ K and the critical pressure is $P_{cr} = 63$ atm), lower alcohols are finding increasing application as supercritical solvents.

An analysis of the literature demonstrates that the thermal isomerization of monoterpenic compounds in supercritical solvents was not studied earlier. There have been only sparse reports on the catalytic hydrogenation of α-pinene in supercritical CO_2 [39–41] and on the synthesis of esters (esterification reactions) of terpenic alcohols [38].

Now we will proceed with a detailed presentation of our studies of the heat-induced conversions of monoterpenic and terpenic compounds in supercritical fluids as solvents [40–48]. It seems pertinent to begin with systematically describing our experimental procedures, data analysis and processing techniques, and reaction scheme and kinetic model construction. We will report the phase states of alcohol–water–α-pinene mixtures (liquid–vapor, liquid–liquid, or liquid–liquid–vapor) studied by methods of nonideal thermodynamics in wide composition, temperature, and pressure ranges—data that can be interesting and significant from the practical standpoint.

EXPERIMENTAL PROCEDURES AND CHEMICAL ANALYSIS OF REACTION PRODUCTS

The following terpenes were used in our experiments: (+)-α-pinene (>98%, Aldrich), (–)-β-pinene (≥99%, Fluka), (+)-limonene (≥99%, Aldrich), (S)-*cis*-verbenol (95%, Aldrich). Sulfate turpentine was a commercial product consisting of α-pinene (76–80%), camphene (1.2%), β-pinene (4.1%), 3-carene (10.8%), limonene (3%), and other compounds (0.9%).

The thermal isomerization of terpenes in supercritical solvents was studied using a laboratory setup with a tubular flow reactor ~7 cm^3 in volume. The reaction temperature and pressure were varied between 530 and 700 K and between 80 and 300 atm, respectively. Depending on the solvent, the reaction mixture was fed into the reactor as one or two liquid streams. In the latter case, one feed was a solution of a monoterpene in an alcohol and the other was distilled water. These independent liquid feeds were mixed at the reactor inlet.

The residence time (τ), defined as the ratio of the reactor volume (V_r) to the flow rate of the reaction mixture (Q_{mix}) under the inlet conditions (T_0, P_0), $\tau = V_r/Q_{mix}$, was ~70–140 s.

The reaction mixture leaving the reactor was cooled and, after separation into gas and liquid phases, was analyzed. The composition of the reaction products was determined by GC-MS on a Hewlett Packard 5890/II gas chromatograph coupled with an HP MSD 5971 quadrupole mass spectrometer as the detector. An HP-5 quartz column (length of 30 m, inner diameter of 0.25 mm, stationary phase: biphenyl (5%)–dimethylsiloxane (95%) copolymer, film thickness of 0.25 μm) was used in these measurements. The carrier gas was helium (1 ml/min). The injection port temperature was 280°C. The oven temperature was programmed as follows: 50°C (2 min), 50–200°C (4°C/min), 200–300°C (20°C/min), and 300°C (20 min). The ionizing electron energy was 70 eV.

Qualitative analyses of reaction products were carried out by comparing the retention (Kovats) indexes and complete mass spectra of components with the

corresponding data for pure compounds (if available) and with mass spectrometric data from the NIST Mass Spectral Library (190825 compounds), Wiley Registry of Mass Spectral Data (621600 compounds), and the catalogue by Tkachev [49]. The percentages of mixture components were derived from chromatographic peak areas without using correction coefficients.

The enantiomer composition of the initial compounds and thermolysis products was determined by GC-MS on an Agilent 6890 gas chromatograph with a 5975 Inert quadrupole mass-selective detector. Mixtures were separated under the following conditions: 30-m-long capillary column; inner diameter of 0.25 mm; CycloSil-B chiral stationary phase with a film thickness of 0.25 μm; helium (1 ml/min) as the carrier gas; injection port temperature of 250°C; interface temperature of 250°C; ion source temperature of 230°C; temperature programming: 50°C (2 min), 50–180°C (2°C/min), 180–220°C (5°C/min), 220°C (20 min); ionizing electron energy of 70 eV; mass scanning range of 29–500 amu. The cathode was switched on 3.5 min after sample injection. The sample size was 0.2 μl.

MATHEMATICAL METHODS OF DATA PROCESSING AND KINETIC SIMULATION

As a rule, kinetic studies of complex reactions in plug-flow reactors result in the establishment of a relationship between the composition of the reaction mixture and the residence time under isothermic and isobaric conditions at a given feed composition. The resulting integral composition–residence time curves are sufficiently informative to postulate some interconversion network and to formulate primary hypotheses concerning the form of the kinetic functions to be fitted to the observed rates of particular reactions. Subsequent processing of the experimental data is performed to determine the numerical values of constants in the rate equations. In order to establish the temperature dependences of these constants, it is necessary to obtain several composition–residence time isotherms at high and low temperatures. A drawback of this approach is that experimental limitations do not allow the residence time (flow rate) at each particular temperature point to be varied in a sufficiently wide range. As a consequence, it is difficult to record complete composition–residence time curves both at comparatively low and at comparatively high temperatures. For this reason, we varied the reaction temperature at a fixed residence time and pressure in most kinetic experiments. Data processing demonstrated that the resulting composition–temperature relationships are informative for the reaction scheme chosen, affording correct temperature-dependent kinetic constant data.

Mathematical Description of the Experimental Reactor

The mathematical model of a plug-flow reactor is represented as the set of ordinary differential equations

$$\frac{dC_i}{d\tau} = \sum_{j=1}^{N_R} z_{ji} R_j(C) \quad (1)$$

subject to the initial conditions

$$\tau = 0: \quad C_1 = C_1^0; \quad C_i^0 = 0, \quad i = 2, \ldots, N_S. \quad (2)$$

Here, C_i^0 designates the inlet component concentrations (g mol/l), N_S is the number of components, N_R is the number of chemical reactions included in the conversion network, and z_{ji} designates the jth row and ith column of the stoichiometric matrix corresponding to the accepted reaction network.

A preliminary analysis demonstrated that all of the reactions are monomolecular and obey the first-order rate law. By equivalent transformations through the introduction of the dimensionless concentrations $y_i = C_i/C_1^0$, the set of equations (1) in this particular case can be represented as

$$\frac{dy_i}{d\tau} = \sum_{j=1}^{N_R} z_{ji} R_j(y), \quad \tau = 0: y_1^0 = 1, \; y_i^0 = 0, \; i = 2, \ldots, N_S, \quad (3)$$

where R_i designates the first-order reaction rates.

Note that, for reactions of fractional and higher orders, the right-hand side of Eq. (3) will contain C_1^0 or an equivalent quantity, namely, the molar volume of the initial mixture.

The rate constants k_j in Eq. (3) are represented according to the Arrhenius law:

$$k_j = k_{j0} \exp\left(-\frac{E_j}{RT}\right). \quad (3a)$$

The set of equations (3) was used in the identification of parameters of the kinetic model.

Identification of the Kinetic Model

The identification problem includes determination of the unknown rate constants and activation energies ensuring the best fit between experimental and calculated data. For this purpose, we formulate an objective function to be minimized with respect to its parameters:

$$Q = \sum_{k=1}^{N_{exp}} \left(\mathbf{y}_k^{exp} - \mathbf{y}_k^{calc}(\mathbf{p})\right)^T \times \mathbf{W}_k^{-1} \left(\mathbf{y}_k^{exp} - \mathbf{y}_k^{calc}(\mathbf{p})\right) \longrightarrow \min(\mathbf{p}), \quad (4)$$

where $\mathbf{y}_k^{exp}$ is the N_S-dimensional column vector consisting of experimental ith component concentrations measured in the kth run, $\mathbf{y}_k^{calc}$ is the vector of calculated concentrations obtained by integrating the set of differential equations (3) between 0 and τ (s) at the temperature of the kth run (T_k), $\mathbf{W}_k$ is the weight unit matrix, and $\mathbf{p}$ is the N_P-dimensional column vector of sought parameters:

$$\mathbf{p} = \left[k_1^0, k_2^0, \ldots, k_N^0, E_1, E_2, \ldots, E_N\right]. \quad (5)$$

Objective function (4) was minimized by Gauss and Marquardt's classical iteration method [50] with modifications [51] making the iterative procedure much more rapid, reducing the size of the confidence region, and thereby enhancing the statistical validity of the constants. The component concentrations were calculated in each iteration step by numerical integration of the set of differential equations (3) at current values of the constants.

Solving the identification problem was followed by an a posteriori analysis of the statistical validity of the results [52, 53].

KINETICS OF THE THERMAL ISOMERIZATION OF MONOTERPENIC COMPOUNDS IN SUPERCRITICAL SOLVENTS

α-Pinene Isomerization in Supercritical Lower Alcohols

Lower alcohols are widespread solvents for many organic compounds and have a high solvating power, particularly toward polar molecules, with which they form hydrogen bonds. They have comparatively low critical parameters and are thermally stable in their vicinity. In view of this, they are of interest as supercritical solvents for chemical reactions. In our investigation of α-pinene isomerization, we chose the lower alcohols methanol, ethanol, and 1-propanol as supercritical solvents.

Figure 1 plots the α-pinene conversion (curves *1*–*3*) and the yield of the main product, limonene (curves *1'*–*3'*), as a function of the residence time for the reactions carried out in supercritical methanol, ethanol, and 1-propanol at a constant temperature and pressure. Here, the residence time was used as the independent variable because the problem was to carry out a comparative analysis of the α-pinene reactivities in different supercritical solvents at a constant temperature and pressure.

It was found that the reactivity of α-pinene in supercritical alcohols increases with an increasing number of CH groups in the alcohol molecule, the chemical composition of the reaction products is solvent-independent, and none of the supercritical alcohols reacts with α-pinene or its isomerization products.

The slight difference between the selectivities of the reaction in different alcohols is most clearly manifested in the dynamics of accumulation of the totality of minor products and in the limonene concentration dynamics. The largest amounts of by-products are observed in α-pinene isomerization in supercritical 1-propanol. The maximum attainable limonene concentration in this solvent is the lowest among the alcohols examined.

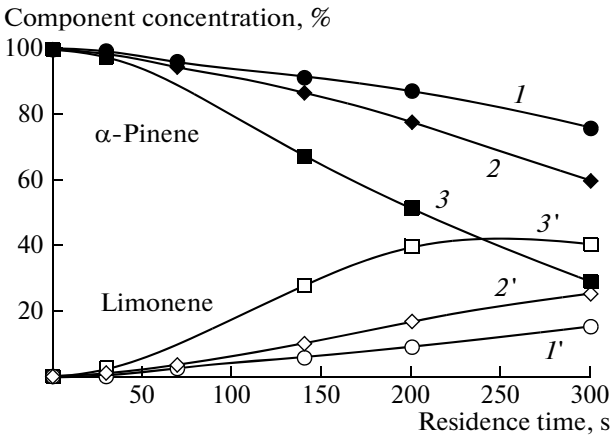

Fig. 1. (*1*–*3*) α-Pinene and (*1'*–*3'*) limonene concentrations in the products of α-pinene isomerization in supercritical alcohols ((*1*) methanol, (*2*) ethanol, and (*3*) 1-propanol) as a function of the residence time (300°C, 100 atm).

No compounds indicating alcohol decomposition were detected among the reaction products. Therefore, all of the alcohols are thermally stable in the temperature and pressure ranges examined.

Although α-pinene proved much more reactive in 1-propanol, we chose supercritical ethanol as the solvent for subsequent kinetic studies of monoterpene isomerization.

α-Pinene Isomerization in Supercritical Ethanol

The experimental data concerning the thermal isomerization of α-pinene (Table 1) were obtained in two series of experiments. The first series demonstrated how the composition of the reaction mixture varies over the temperature range of 560–660 K at a constant pressure of $P = 120$ atm and a constant residence time of $\tau = 70$ s. The second series of experiments was carried out to elucidate the effect of the reaction medium pressure on the α-pinene conversion rate at a constant temperature of 600 K and a constant residence time of $\tau = 70$ s.

Figure 2 shows the temperature dependence of the reaction mixture composition in thermal α-pinene isomerization at a constant pressure (points) based on the data presented in Table 1. Our experimental data and an analysis of the literature [13, 14, 16, 23] suggest that the main routes of α-pinene isomerization in supercritical alcohols can be represented as Scheme 1, which is similar to the scheme of α-pinene isomeriza-

Table 1. Experimental data on the thermal isomerization of α-pinene in supercritical ethanol at a constant residence time of $\tau = 70$ s

T, K	P, atm	Reaction mixture composition normalized to the initial α-pinene concentration, %					
		α-pinene	limonene	4*E*,6*Z*-alloocimene	4*E*,6*E*-alloocimene	(α + β)-pyronene	other products
561	120	82.8	11.5	2.6	2.1	0.2	0.8
581		60.4	23.0	10.3	5.0	0.8	0.5
601		32.1	37.4	18.3	9.4	2.1	0.7
621		5.6	52.5	21.9	13.1	6.2	0.7
641		1.0	49.0	21.4	10.5	13.8	4.3
661		0.9	48.1	11.5	5.6	26.0	7.9
600	90	49.4	28.2	14.0	6.2	1.4	0.8
	120	32.1	37.4	18.3	9.4	2.1	0.7
	150	16.1	45.7	20.7	13.2	3.3	1.0
	180	10.4	48.3	24.2	12.2	4.2	0.7
	210	6.4	49.3	25.7	12.7	4.7	1.2
	270	3.3	52.2	20.3	16.5	5.7	2.0

tion in the gas or liquid phase [13, 14, 16, 23]. The rate of each step obeys a first-order rate equation.

The occurrence of reversible conversions between the 4*E*,6*Z*- and 4*E*,6*E*-alloocimenes is proved by the fact that the concentration ratio of these two isomers in the reaction products (Table 1) is nearly the same, approximately 2, at all experimental temperatures. These reversible reactions are rapid, and this is why the rate constants of steps 4 and 5 cannot be identified. This provides good reason to simplify the model: these isomers are taken to be a single component (4*E*,6*Z*- and 4*E*,6*E*-alloocimenes), and the concentration of this component is taken to be equal to the sum of the isomer concentrations.

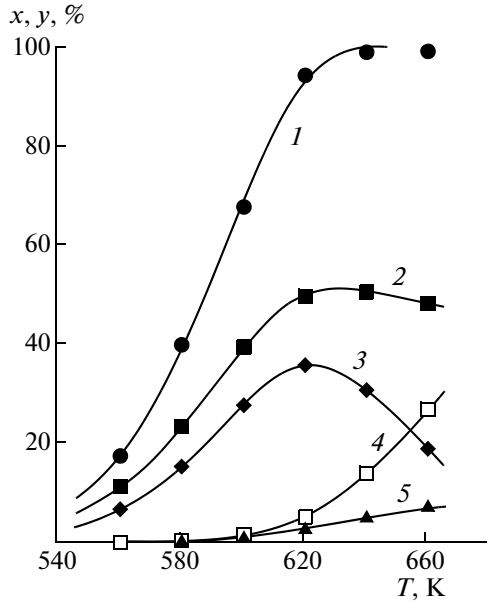

Fig. 2. α-Pinene conversion and isomerization product yields as a function of temperature ($P = 120$ atm, $\tau = 70$ s): (*1*) α-pinene, (*2*) limonene, (*3*) 4*E*,6*Z*-alloocimene, (*4*) 4*E*,6*E*-alloocimene, and (*5*) pyronene isomers. The points represent experimental data, and the solid lines represent calculated data.

The minimization of the objective function (4) for the model based on the complete network of α-pinene thermal isomerization reactions (Scheme 1) enabled us to calculate kinetic parameters (rate constants and activation energies) and their confidence intervals. In spite of the good agreement between the experimental and calculated data, all parameters of the kinetic model (except for routes 1 and 2 in Scheme 1) contain large uncertainties. This is evident from their wide confidence intervals corresponding to the 95% confidence level, which far exceed the rate constant estimates in some cases. Obviously, the experimental data are indifferent to these routes.

Based on these considerations, we suggest a simplified reaction network (Scheme 2). The results of the identification of this model as calculated constants and their confidence intervals are presented in Table 2. Figure 2 demonstrates that the experimental and calculated data in this case are in good agreement.

Although the rate constant k_{40} has a wide confidence interval, route 4 in Scheme 2 was not excluded

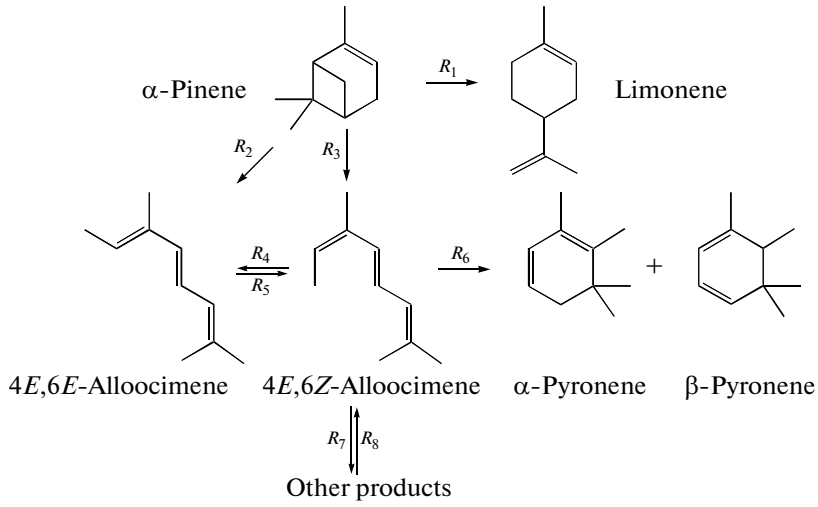

The other products include the dimerization and polymerization products of alloocimenes, [4+2]-cycloaddition products, etc.

Scheme 1. Complete scheme of α-pinene thermal isomerization routes.

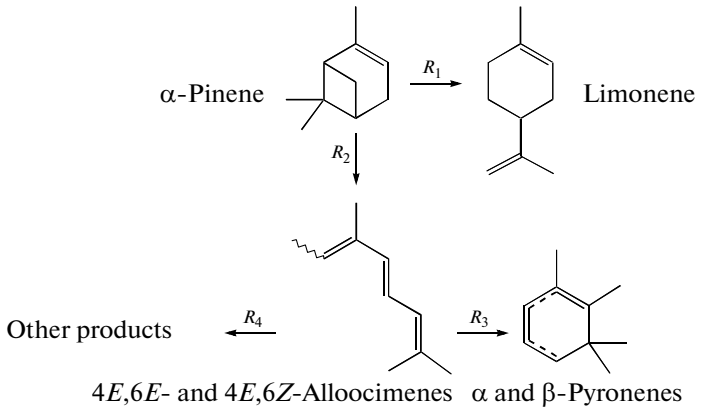

Scheme 2. Simplified scheme of α-pinene thermal isomerization routes.

from the model, because doing this would break the balance in the system.

Selectivity of the reaction. Figure 3 plots the temperature dependences of the reaction selectivities with respect to the main products. Here, selectivity is an integral quantity defined as the ratio of the isomerization product yield to the amount of converted α-pinene under given conditions. As in the case of the gas- or liquid-phase thermal isomerization, the main product of α-pinene conversion in supercritical ethanol is limonene. The limonene selectivity of the reaction decreases with increasing temperature because the activation energy of route 2 is higher than that of route 1: $E_2 > E_1$ (see Eq. (6)).

$$S_{\mathrm{Li}} = \frac{k_1}{k_1 + k_2} = \frac{k_{10}\exp(-E_1/RT)}{k_{10}\exp(-E_1/RT) + k_{20}\exp(-E_2/RT)}. \quad (6)$$

As a consequence, raising the reaction temperature is favorable for route 2 (Scheme 2), increasing the yield of the alloocimene isomers. As the temperature is further increased, the overall α-pinene conversion begins to be dominated by the reactions yielding pyronene

Table 2. Estimates of the kinetic constants of the reactions in Scheme 2 and their statistical characteristics

Kinetic constants and their confidence intervals			
rate constant, s^{-1}		activation energy, kJ/mol	
k_{10}	8.51E+07 ± 1.38E+07	E_1	118.0 ± 8.07
k_{20}	2.73E+09 ± 4.99E+08	E_2	137.0 ± 9.21
k_{30}	1.08E+08 ± 6.15E+07	E_3	129.0 ± 31.0
k_{40}	1.23E+03 ± 1.37E+03	E_4	74.3 ± 60.6
Standard error			0.97%

isomers and other by-products, thus reducing the total alloocimene selectivity.

For convenient comparison between the α-pinene isomerization rate in supercritical ethanol with the same data for the gas and liquid phases from the literature, we will consider the overall rate of α-pinene isomerization via all routes. As follows from Fig. 4, the overall rate of α-pinene isomerization in supercritical ethanol is well above the rates of isomerization in the gas and liquid phase. At the same time, the observed activation energies of these reactions are approximately equal, and this fact should be taken into consideration when comparing the activation energies of isomerization of other monoterpenic compounds (β-pinene, verbenol, and turpentine) in supercritical ethanol under equal conditions. Such a comparison would provide a better understanding of the common and specific features of the reactions of structurally similar compounds in supercritical solvents and would demonstrate the potential of solvents for selectivity and reaction rate control.

α-Pinene Isomerization in Water-Containing Supercritical Ethanol

Interest in the thermal isomerization of α-pinene in supercritical ethanol–water mixtures (in our study, monoterpene isomerization was carried out in ethanol containing ~5% water) stems from the desire to understand the effect of water on the reaction mechanism and on the selectivity and rate of the overall conversion. This is explained by the fact that water in the region of its critical parameters (SCW) is strongly dissociated [54, 55] and can show the properties of an acid or base catalyst. This is favorable for a variety of chemical reactions [36, 37]. However, as was found experimentally, use of pure SCW as a solvent in the thermal isomerization of α-pinene causes deep structural rearrangements of the terpene into 60 identified products because of the high reactivity of SCW. The carbon backbones of the products vary between C_6 and C_{40} and are dominated by C_{10} (monoterpenic compounds). The main α-pinene conversion product under these conditions is limonene, whose yield does not exceed 20–25%. Bringing the solvent (water) into the subcritical region effects limonene hydration into the monoterpene alcohol α-terpineol (~20–25%).

Experimental data on the thermal isomerization of α-pinene in supercritical ethanol–water mixtures are presented in Fig. 5 (points) as the dependence of the mole fractions of reaction products (limonene, alloocimene isomers, pyronenes, and the total fraction of other products) on the water content of the feed under fixed conditions. It follows from these dependences that, in spite of the high water concentration in ethanol, the distribution of α-pinene isomerization products is the same as in the case of thermal isomerization in pure supercritical ethanol (Table 1). Furthermore, as the water concentration in the reaction mixture is raised, the limonene yield increases from 57 to 69%,

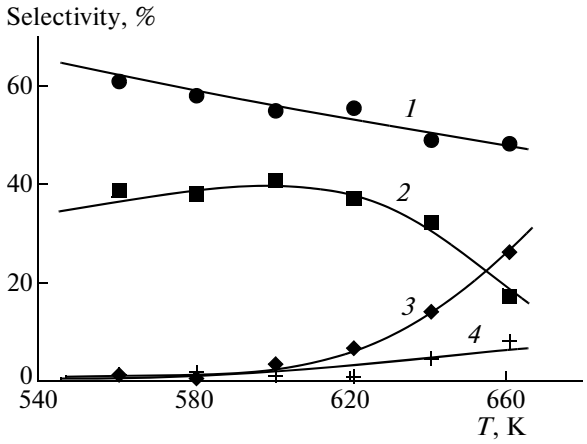

Fig. 3. Product selectivities as a function of temperature: (*1*) limonene, (*2*) 4*E*,6*Z*- and 4*E*,6*E*-alloocimenes, (*3*) (α + β)-pyronenes, and (*4*) other products.

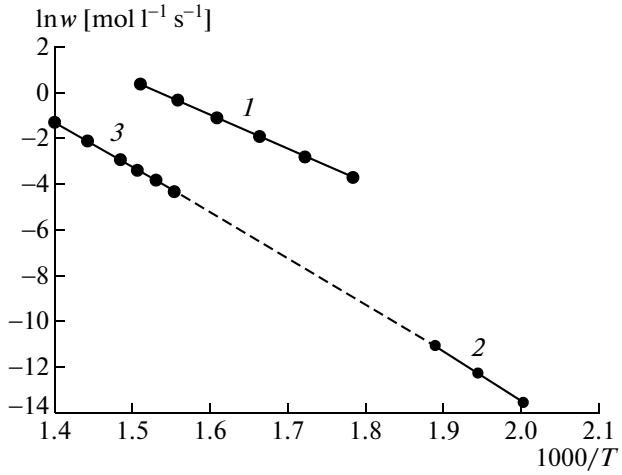

Fig. 4. Arrhenius plot of the overall rate of the thermal isomerization of α-pinene (*1*) in supercritical ethanol, (*2*) in the liquid phase [16], and (*3*) in the gas phase [18, 19].

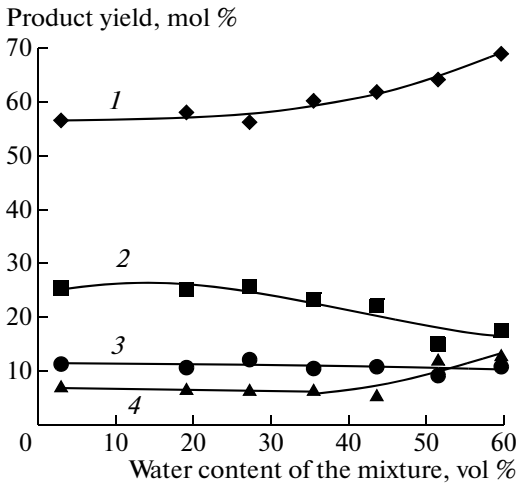

Fig. 5. Yields of organic products as a function of the water content of the reaction mixture: (*1*) limonene, (*2*) 4*E*,6*Z*- and 4*E*,6*E*-alloocimenes, (*3*) pyronenes, and (*4*) other products. The concentrations are normalized to the initial α-pinene concentration in the solution. $T = 657$ K; $P = 230$ atm.

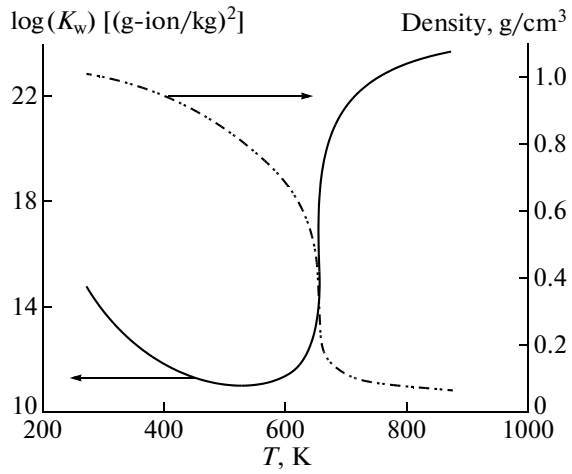

Fig. 6. Negative logarithm of the water ion product and water density as a function of temperature at $P = 230$ atm.

the yield of alloocimene isomers remains almost unchanged, and the pyronene concentration decreases markedly, possibly because of the increasing yield of other products. As the water concentration in the reaction mixture is lowered, the qualitative and quantitative compositions of the α-pinene isomerization products tend to those typical of isomerization in pure supercritical ethanol. Therefore, the increase in the limonene yield with an increase in the water concentration in the supercritical solvent can be due to the increasing contribution from the ionic mechanism of α-pinene isomerization.

Indeed, as was noted above, as the density of the supercritical medium increases in the critical region of water parameters, the H^+ ion concentration grows considerably owing to the increasing degree of ionization of water [54, 55]. This imparts water the properties of an acid catalyst and can thus increase the reaction rate [56, 57]. In order to obtain a quantitative estimate of the degree of ionization of water in a supercritical water–ethanol mixture (and, accordingly, the H^+ and OH^- concentrations), it is necessary to correctly calculate the ionization constants of subcritical and supercritical water as a function of temperature, pressure (density), and the fraction of water in the two-component supercritical solvent.

As a rule, the degree of ionization of water is characterized by the ion product $K_w = [H^+] \times [OH^-]$. Under normal conditions, $\log K_w = -14$. As the temperature is raised to 800°C at a density of 1 g/cm^3, the water ion product increases by 6 orders of magnitude and the H^+ concentration increases by 3 orders of magnitude [54].

In this study, K_w was calculated using the empirical equation suggested in [55], which is valid in the temperature range of 273–1273 K and in the pressure range of 1–10000 atm:

$$\log K_w = Q_1(T) + Q_2(T)\log\rho_w,$$
$$Q_1 = A + B/T + C/T^2 + D/T^3, \quad (7)$$
$$Q_2 = E + F/T + G/T^2.$$

Here, K_w is expressed in units of (g-ion/kg)^2 and the water density ρ_w is expressed in units of g/cm^3. The coefficients of Eq. (7) are as follows [55]:

$A = -4.098$; $B = -3245.2$ K; $C = 2.2362 \times 10^5$ K^2;
$D = -3.984 \times 10^7$ K^3; $E = 13.957$;
$F = -1262.3$ K; $G = 8.5641 \times 10^5$ K^2.

Figure 6 plots the temperature dependence of the ion product and density of water at $P = 230$ atm as calculated via Eq. (7). The density of water was calculated according to NIST standards [58]. It is clear from Fig. 6 that the water ion product increases by 3 orders of magnitude as the temperature is raised from 300 to 600 K. As water reaches its critical point and passes into the supercritical state in the 600–700 K interval, K_w decreases sharply because of the water density decreasing in this temperature range.

Because isomerization was performed in water–alcohol mixtures (solutions), in the calculation of K_w via Eq. (7) the density of pure water, ρ_w, was replaced with the "density of water in the mixture," $\rho_{w,mix}$:

$$\rho_{w,mix} = \rho_w C_w \ [g_{H_2O}/cm^3_{mix}], \quad (8)$$

where C_w is the volume faction of water in the solution ($cm^3_{H_2O}/cm^3_{mix}$). Although the definition of the "density of water in the mixture" ($\rho_{w,mix}$) in terms of Eq. (8) is somewhat arbitrary, it accounts well for the variation of K_w with the water concentration in the solution.

Scheme 3 depicts the most likely free-radical and ionic mechanisms (routes **A** and **B**, respectively) of α-

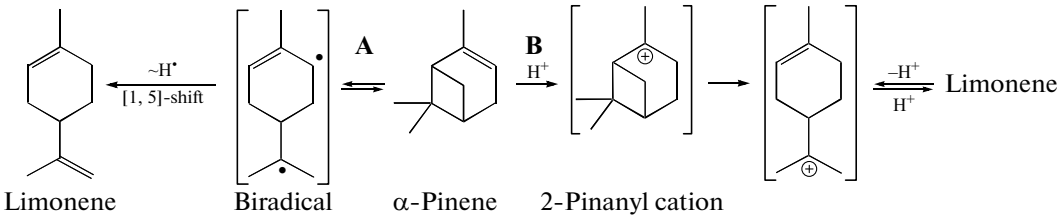

Scheme 3. Free-radical (route **A**) and ionic (route **B**) mechanisms of α-pinene isomerization.

pinene isomerization. The first step of route **A** yields an intermediate biradical with a *p*-menthane structure, which then turns into limonene, formally via the [1,5] shift of the H• atom.

The key step of the ionic mechanism (route **B**) is the formation of a pinane-type carbocation, which, according to the literature [5], forms readily from the α-pinene molecule as a result of electrophilic attack by an H^+ ion. The resulting cation undergoes skeletal rearrangement into a *p*-menthane-type carbocation, which then yields limonene.

Schematically, the elementary steps of the ionic mechanism can be represented as

$$\begin{gathered}\text{(I) } \mathbf{P} + \mathbf{H}^+ \longrightarrow \mathbf{PH}^+; \\ \text{(II) } \mathbf{PH}^+ \longrightarrow \mathbf{LH}^+; \quad \text{(III) } \mathbf{LH}^+ \rightleftharpoons \mathbf{L} + \mathbf{H}^+,\end{gathered} \tag{9}$$

where **P** = α-pinene, **L** = limonene, and $\mathbf{PH}^+$ and $\mathbf{LH}^+$ are the respective intermediate cations. In water–acid solutions, the first step is usually rate-limiting. In addition, step I is likely irreversible: in the presence of an acid, α-pinene undergoes rapid skeletal rearrangements never leaving the pinane backbone intact. By contrast, the *p*-menthane backbone of limonene remains practically unchanged under the same conditions.

Within the simplified scheme of α-pinene conversions (Scheme 2), with the two possible α-pinene isomerization mechanisms (Scheme 3) taken into consideration, the overall limonene formation rate is representable as

$$R_\text{l} = R_{1\text{A}} + R_{1\text{B}}, \tag{10}$$

where $R_{1\text{A}} = k_{1\text{A}}[y_\text{l}]$ is the reaction rate for route **A** and y_l is the mole fraction of α-pinene in the solution. Under the assumption that the rate-limiting step of route **B** is step I of mechanism (9), the reaction rate for route **B** is

$$R_{1\text{B}} = k_{1\text{B}}[y_\text{l}] \times [\text{H}^+], \tag{11}$$

where $[H^+]$ is the H^+ ion concentration in the solution. Steps II and III of mechanism (9) are taken to be reversible reactions with equilibrium constants K_2 and K_3, respectively:

$$K_2 = \frac{[\text{LH}^+]}{[\text{PH}^+]}, \quad K_3 = \frac{[\text{L}][\text{H}^+]}{[\text{LH}^+]}. \tag{12}$$

The reactions of mechanism (9) are supplemented with the solution electroneutrality equation

$$\begin{gathered}[\text{H}^+] + [\text{PH}^+] + [\text{LH}^+] = [\text{OH}^-], \\ \text{where } [\text{OH}^-] = K_\text{w}/[\text{H}^+].\end{gathered} \tag{13}$$

After determining the cation concentrations $[AH^+]$ and $[BH^+]$ from Eq. (12) and substituting these concentrations into Eq. (13), the latter can be solved for $[H^+]$ as

$$\left[\text{H}^+\right] = \sqrt{K_\text{w}/\text{Denom}}, \tag{14}$$

$$\text{Denom} = 1 + \frac{[\text{L}]}{K_3}\left(\frac{1}{K_2} + 1\right). \tag{15}$$

The expression for the reaction rate (11) with Eq. (14) taken into account can be written as

$$R_{1\text{B}} = k_{1\text{B}} y_\text{l} \sqrt{K_\text{w}}/\sqrt{\text{Denom}}. \tag{16}$$

Equation (16) demonstrates that, in principle, limonene accumulation in the reaction products can decrease the limonene formation rate $R_{1\text{B}}$ (because of the increase in the Denom value due to the growth of the limonene concentration [L]). In fact, this does not take place, because the absolute values of the limonene concentration in the supercritical solution are small (≤0.05 wt %). Accordingly, the second term of Eq. (15) is much smaller than unity and Denom ≈1. As a consequence, the rate of limonene formation via the ionic mechanism, $R_{1\text{B}}$, is directly proportional to $\sqrt{K_\text{w}}$.

It would be logical to assume that, in the presence of water, the ionic mechanism can take place for the other products of thermal α-pinene isomerization. If this is the case, the rates of the other reactions appearing in Scheme 2 will also depend on the H^+ concentration and will be proportional to $\sqrt{K_\text{w}}$ (first-order with respect to H^+).

The mathematical model of α-pinene conversions according to Scheme 2 is the following set of ordinary differential equations:

$$\begin{aligned}\frac{dy_1}{d\tau} &= -(k_1 + k_2)y_1\\ \frac{dy_2}{d\tau} &= k_1 y_1\\ \frac{dy_3}{d\tau} &= k_2 y_1 - (k_3 + k_4)y_3\\ \frac{dy_4}{d\tau} &= k_3 y_3\\ \frac{dy_5}{d\tau} &= k_4 y_3,\end{aligned} \quad (17)$$

$$\tau = 0: y_1 = y_1^0, y_2 = y_3 = y_4 = y_5 = 0. \quad (18)$$

The subscripts i in y_i (mole fractions) correspond to the component numbers in Scheme 2.

Since the reaction rate for all routes in Scheme 2 is zero when there is no water in supercritical ethanol (under conditions such that limonene forms largely via the free-radical mechanism), the overall rate constants k_j in model (17) are represented as

$$k_j = k_{jA} + k_{jB}[H^+], \quad j = 1–4. \quad (19)$$

In order to verify the above assumptions, we determined the numerical values of the parameters of model (17) using experimental data. The problem was solved by minimizing the objective function

$$S = \sum_{j=1}^{N_{exp}} \sum_{i=1}^{N_S} \left(y_{ij}^{exp} - y_{ij}^{calc}\right)^2 \longrightarrow \min. \quad (20)$$

Here, $N_S = 5$ is the number of components and $N_{exp} = 8$ is the number of experiments carried out at various water concentrations in the two-component water–alcohol supercritical solvent. The parameters of these experiments are constant values of temperature, pressure, and residence time, as well as H^+ concentrations calculated using the above procedure for the preset water concentration in each particular experiment. The minimization problem was solved by the combined, direct/indirect, gradient method [59]. The essence of this method is that calculated concentration values (y_{ij}^{calc}) are found as the integrals of the right-hand sides of Eq. (17):

$$y_{ij}^{calc} = y_i^0 + \int_0^\tau \Phi_i\left(\mathbf{y}, \mathbf{k}, [H^+]\right)d\tau. \quad (21)$$

Here, Φ_i (y, k, $[H^+]$) stands for the corresponding right-hand sides of the differential equations (17). The integrals in expression (21) were calculated by the method described in [59]. This method proved more reliable than the implicit method suggested in [60], which is based on y_{ij}^{calc} calculation by integrating the set of equations (17), because the objective function formulated in terms of integrals in (21) is a quadratic function of unknown parameters. Due to this circumstance, the size of the confidence region of the parameters is much smaller and, accordingly, their statistical validity is higher. The objective function in the implicit method, which uses the numerical or analytical solution of the set of equations (17) in y_{ij}^{calc} calculation, is strongly nonlinear with respect to the sought parameters. As a consequence, the confidence region size is much larger and, accordingly, the statistical validity of the parameters is lower.

Table 3. Rate constant data

Constant	Units	Value
k_{1A}	s^{-1}	$(8.9 \pm 1.5) \times 10^{-2}$
k_{2A}		$(6.8 \pm 1.1) \times 10^{-2}$
k_{3A}		$(1.7 \pm 0.3) \times 10^{-2}$
k_{4A}		$(3.9 \pm 0.8) \times 10^{-3}$
k_{1B}	kg (g-ion s)$^{-1}$	$(5.9 \pm 2.9) \times 10^{+8}$
k_{2B}		$(1.1 \pm 0.5) \times 10^{+8}$
k_{3B}		$(4.0 \pm 1.6) \times 10^{+7}$
k_{4B}		$(3.8 \pm 0.3) \times 10^{+6}$
Standard deviation between the experimental and calculated data, %		1.74

The calculated rate constants are listed in Table 3. Clearly, the values of all rate constants are well-conditioned, with acceptable confidence intervals. The standard deviation between the experimental and calculated data is below 2%. The fit between the experimental and calculated data is illustrated by Fig. 7, which plots the yields of the main reaction products versus the H^+ concentration in the supercritical water–alcohol solvent. Here, the solid lines represent the calculated values obtained by integrating the set of equations (17) and the points represent experimental data. It is clear from Fig. 7 that the model with these calculated rate constants is in good agreement with the experimental data.

The limonene, alloocimene, and by-product formation reactions turned out to be the most sensitive to the H^+ concentration in the solvent. While the alloocimene yield decreases with increasing $[H^+]$, the yields of limonene and by-products rise. For example, the limonene yield can increase by 10–15% as the water concentration in the supercritical water–ethanol mixture is raised from 0 to 60 vol %. However, taking into account the results of thermal α-pinene isomerization in pure SCW (discussed above), it can be deduced that, upon further increase in the water concentration (and,

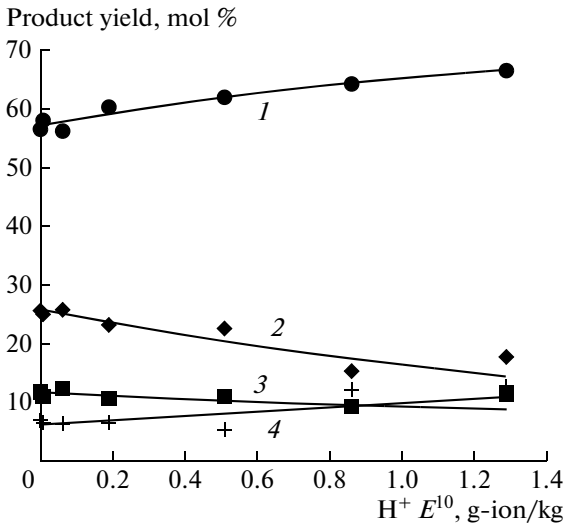

Fig. 7. Yields of main products as a function of the H^+ ion concentration in the supercritical water–ethanol solvent (T = 657 K, P = 230 atm, τ = 70 s): (*1*) limonene, (*2*) alloocimenes, (*3*) pyronenes, and (*4*) other products. The solid lines represent calculated data, and the points represent experimental data.

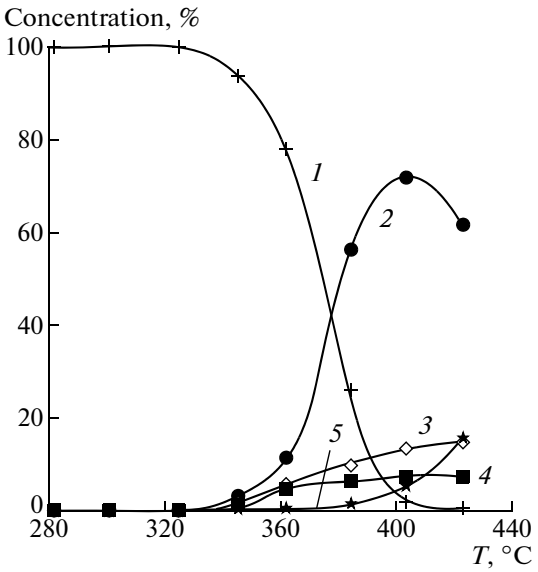

Fig. 8. Concentrations of β-pinene and its isomerization products as a function of temperature (P = 120 atm, τ = 70 s): (*1*) β-pinene, (*2*) β-myrcene, (*3*) limonene, (*4*) *p*-mentha-1(7),8-diene, and (*5*) other products. The solid lines represent the data calculated using the model, and the points represent experimental data.

accordingly, the H^+ concentration) in the reaction mixture, the limonene yield will stop increasing and will begin to decline and other compounds will dominate the conversion products.

One of the most important results of this study is that it verified the assumption that, in the presence of water, the electrophilic (ionic) mechanism of thermal α-pinene isomerization can be "switched on" to join the radical mechanism. The electrophiles are H^+ ions, whose concentration increases dramatically in the critical region owing to the increasing degree of ionization of the H_2O molecules.

Isomerization of β-Pinene and the α- + β-Pinene Mixture in Supercritical Ethanol

β-Pinene is an isomer of α-pinene. The molecules of both compounds have the same carbon backbone and differ only in the position of the C=C bond. In the gas phase, β-pinene, like α-pinene, undergoes thermal rearrangement, whose main product is β-myrcene. It is interesting to compare the reactivities of these pinenes and the kinetics of their conversion in supercritical ethanol under equal conditions.

We studied the effect of temperature in the 280–420°C range on the β-pinene conversion and thermolysis selectivity in supercritical ethanol at P = 120 atm and τ = 70 s. Experiments demonstrated that the β-pinene conversion in supercritical ethanol is over 99% even at 410°C (Fig. 8). The main reaction of β-pinene in supercritical ethanol is its thermolysis, as in the case of α-pinene [42, 43], which yields a mixture of monocyclic and acyclic compounds with the general formula $C_{10}H_{16}$. Here, the products of β-pinene conversion are the same as in the thermal isomerization of β-pinene in the gas or liquid phase [8, 18, 19, 26, 61, 62]. The identity of the products of β-pinene conversion in supercritical ethanol and the products of thermal β-pinene isomerization in the gas phase suggests that the β-pinene thermolysis mechanism in supercritical ethanol and in the gas phase is the same (Scheme 4). This mechanism includes the formation of the intermediate biradical I, which then either turns into limonene and *p*-mentha-1(7),8-diene or transforms into biradical II, finally yielding β-myrcene.

It was demonstrated that, under our experimental conditions, the main β-pinene conversion routes are the following reactions:

$$\begin{aligned}
&1.\ \beta\text{-pinene} \xrightarrow{R_1} \text{limonene},\\
&2.\ \beta\text{-pinene} \xrightarrow{R_2} \beta\text{-myrcene},\\
&3.\ \beta\text{-pinene} \xrightarrow{R_3} p\text{-mentha-1(7),8-diene},\\
&4.\ \beta\text{-myrcene} \xrightarrow{R_4} \text{other products}.
\end{aligned} \qquad (22)$$

The main reaction of β-pinene in supercritical ethanol is the thermal opening of the bicyclic pinane system yielding acyclic β-myrcene, whose maximum yield (72%) is reached at 400°C (Table 4). As the temperature is further raised, the yield of this product decreases markedly and the yields of other products, mainly oligomers with unidentified structures, increase sharply. These temperature dependences of the accumulation of unidentified products and of the β-myrcene yield suggest that the main contribution to

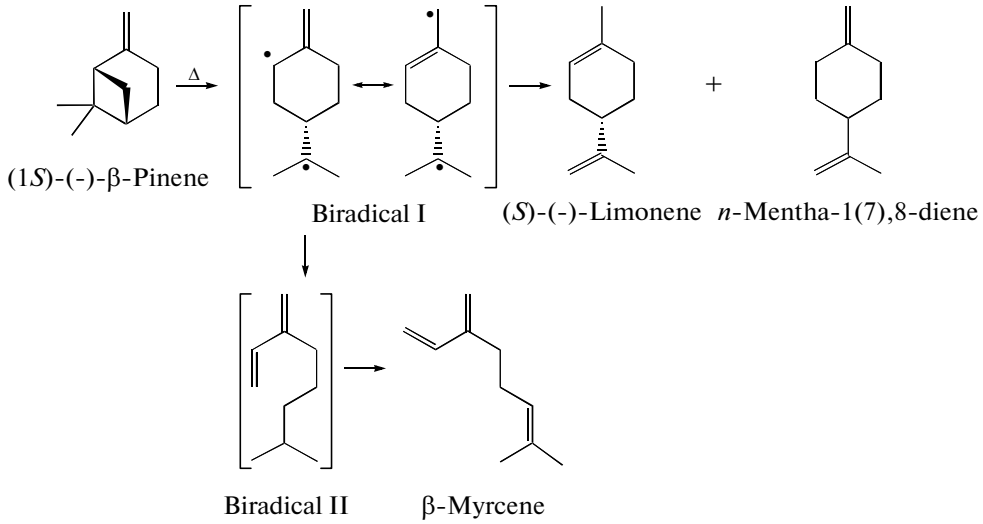

Scheme 4. Mechanism of the thermal isomerization of β-pinene in supercritical ethanol.

the formation of the unidentified products is from reactions of β-myrcene, such as [4+2]-cycloaddition [63] and polymerization [64].

The enantiomer composition of the products resulting from the thermolysis of α-pinene or β-pinene alone in supercritical ethanol [47] indicates that there is a single possible route for limonene forming directly from β-pinene. *p*-Mentha-1(7),8-diene, α-pinene and β-myrcene cannot be limonene precursors in β-pinene thermolysis. In addition, the conservation of the initial enantiomer purity of β-pinene during its thermolysis rules out the occurrence of reversible steps for reactions 2 and 3 in the reaction scheme (22). There is no reversibility in the β-pinene ⟶ limonene reaction as well, as is indicated by the fact that even traces of β-pinene were not observed in limonene thermolysis in supercritical ethanol [43]. It is, therefore, possible to substantially reduce the number of elementary reactions in the kinetic model.

The β-pinene thermal conversion scheme (22) was used as the basis for the kinetic model. The rate constants obtained by identification of this model are statistically reliable. The numerical values of the rate constants of the reactions appearing in scheme (22) are listed in Table 5. Figure 8 presents a comparison between the calculated and experimental data, demonstrating that the accepted kinetic model is in good agreement with the experimental data.

A comparison between the specific overall rate of β-pinene isomerization in supercritical ethanol and the same data for gas-phase isomerization [18, 19, 26, 62] (Fig. 9) indicates that the gas-phase reaction is initiated at lower temperatures than the reaction in supercritical ethanol. In addition, the specific rate of β-pinene isomerization in supercritical ethanol is several orders of magnitude higher than that observed in the gas phase and the activation energy of the reaction in supercritical ethanol at $P = 120$ atm far exceeds that of the gas-phase reaction at $P \le 1$ atm in all of the three cases considered.

Isomerization of the α- + β-pinene mixture in supercritical ethanol. The products of the cothermoly-

Table 4. Outcomes of β-pinene isomerization in supercritical ethanol as a function of temperature (residence time of 70 s, $P =$ 120 atm, $C_0 = 1$ mol/l)

Component, %	Temperature, °C							
	280	300	320	340	360	380	400	420
β-Pinene	100.0	100.0	99.7	93.6	77.6	25.8	1.9	0.6
(±)-Limonene	–	–	–	1.6	5.8	10.0	13.3	14.7
β-Myrcene	–	–	0.1	3.5	11.5	56.4	71.9	61.6
p-Mentha-1(7),8-diene	–	–	–	1.0	4.6	6.2	7.5	7.3
Other products	–	–	0.2	0.3	0.5	1.6	5.4	15.8

Table 5. Calculated parameters of the kinetic model of the thermal conversions of β-pinene

Reaction	Thermolysis in the vapor phase at $P = 1$ atm		Thermolysis in supercritical ethanol at $P = 120$ atm	
	k_0 (s^{-1})	E_a (kJ/mol)	k_0 (s^{-1})	E_a (kJ/mol)
β-Pinene ⟶ β-myrcene	5147.0 ± 97.0	77.6 ± 1.78	$(1.31 \pm 0.27) \times 10^{20}$	276.1 ± 16.7
β-Pinene ⟶ limonene	564.6 ± 42.5	76.8 ± 7.36	$(2.07 \pm 0.43) \times 10^{19}$	275.3 ± 17.5
β-Pinene ⟶ *p*-Menthadiene	605.2 ± 99.3	82.2 ± 16.15	$(2.64 \pm 0.60) \times 10^{14}$	215.3 ± 19.2
β-Myrcene ⟶ other products	581.5 ± 40.2	75.1 ± 6.95	$(2.32 \pm 0.87) \times 10^{8}$	15.76 ± 3.28
Standard error	1.11%		1.08%	

sis of the equimolar α- + β-pinene mixture consist only of the compounds that result from the independent thermolysis of individual α-pinene [42, 46] and β-pinene [47] in supercritical ethanol. The reaction mixture contained no compounds that could have resulted from the interaction between α- and β-pinene thermolysis products or from the interaction of these products with either pinene. For this reason, in the mathematical description of the cothermolysis of the equimolar α- + β-pinene mixture, routes 1–4 of scheme (22) and the α-pinene thermolysis reactions in supercritical ethanol (Scheme 2) were left as the basis of the kinetic scheme. Accordingly, the general scheme of heat-induced reactions of the α- + β-pinene mixture in supercritical ethanol can be represented as Scheme 5.

The thermolysis rate constants of β-pinene nixed with α-pinene, obtained by identification of the kinetic model based on Scheme 5, coincide, within the confidence interval, with the rate constants derived from experimental data for individual β-pinene. This is further evidence that, under the given experimental conditions, α-pinene and β-pinene undergo thermolysis independently, even though they yield the same products, namely, limonene and a group of compounds that were given the common name of "other products." The good agreement between the experimental data and the corresponding calculated data for all reaction participants (Figs. 10, 11) is evidence that the parameters of the kinetic model were calculated correctly.

Note that, in addition to the reactions appearing in Scheme 5, the reversible prototropic isomerization reaction α-pinene ⇌ β-pinene was included in the kinetic model of the overall cothermolysis process. This reaction could occur in supercritical ethanol under the thermal conditions of our experiment, as was suggested by earlier results [65, 66]. However,

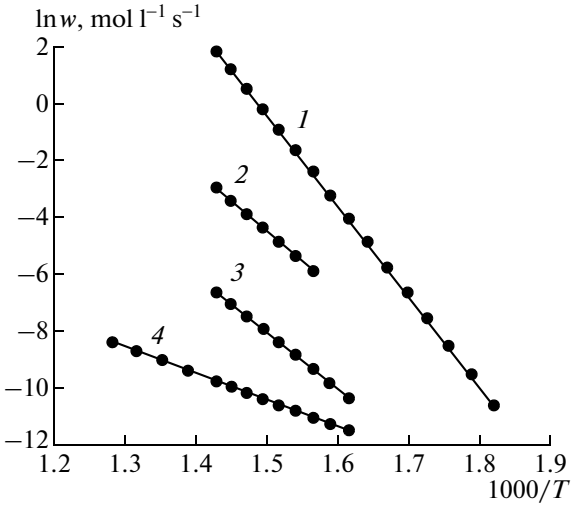

Fig. 9. (*1*) Specific overall rate of thermal isomerization of β-pinene in supercritical ethanol compared to (*2–4*) literature data: (*2*) [18, 19], (*3*) [62], and (*4*) [26].

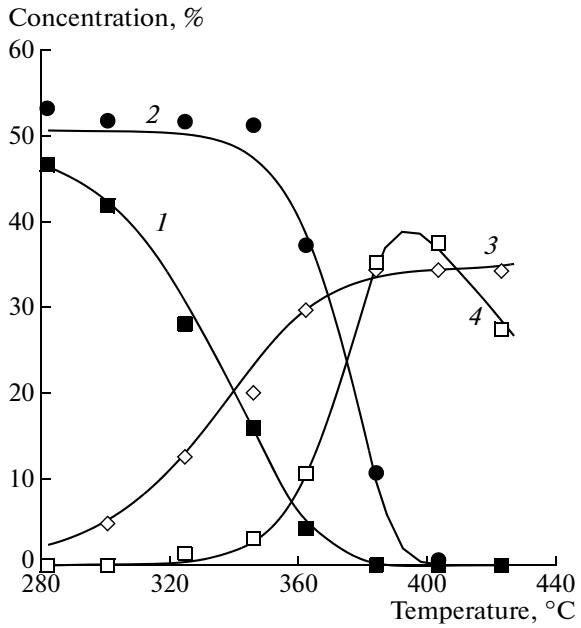

Fig. 10. Comparison between experimental and calculated data: (*1*) α-pinene, (*2*) β-pinene, (*3*) limonene, and (*4*) β-myrcene. The lines represent the data calculated using the model, and the points represent experimental data.

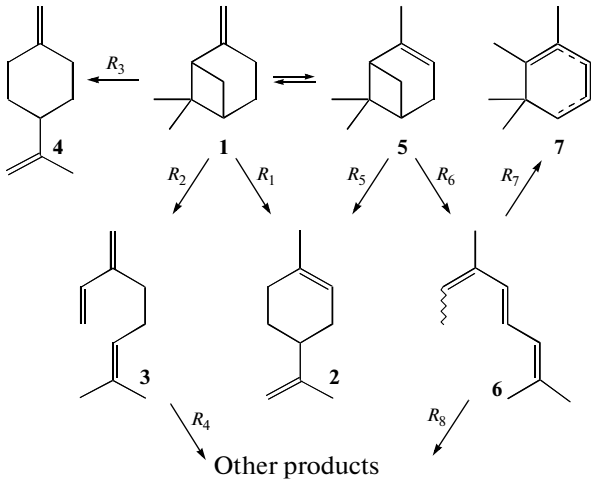

1, β-Pinene
2, Limonene
3, β-Myrcene
4, *n*-Menthadiene
5, α-Pinene
6, Alloocimene
7, Pyronenes

Scheme 5. General scheme of the thermal isomerization of α- and β-pinenes.

model identification did not confirm the occurrence of the forward or back reaction; therefore, under the given experimental conditions, the interconversion of α-pinene and β-pinene proceeds much more slowly than their conversion into other products. This inference is corroborated by the following experimental data. Firstly, α-pinene thermolysis does not yield β-myrcene, the main product of β-pinene thermolysis. Secondly, the limonene resulting from β-pinene thermolysis has the same enantiomer purity as the initial β-pinene. This means that the β-pinene ⟶ α-pinene reaction does not occur during thermolysis, since α-pinene would turn into racemic limonene (dipentene) [47], which would reduce the enantiomer purity of the limonene resulting from enantiomerically homogeneous β-pinene.

Note also the fact that β-pinene conversion starts at higher temperatures than α-pinene thermolysis and its rate increases more rapidly with increasing temperature. Among the basic reactions involving α-pinene and β-pinene (Tables 2, 5), those of β-pinene are characterized by higher activation energies and preexponential factors. This can clearly be seen from the plots presented in Fig. 10 and from the dependences of the overall rates of thermal α-pinene and β-pinene isomerizations (Figs. 4, 9).

Thermolysis of Sulfate Turpentine at High Pressures

As was mentioned above, α-pinene is the main component (up to 80%) f sulfate turpentine. The high α-pinene concentration (~5.0 mol/l) allows one to draw analogies and make comparisons between the thermal isomerization of turpentine and that of pure α-pinene under various conditions, including in supercritical solvents. At the same time, the difference between the α-pinene concentrations in turpentine and in the related systems, the presence of other terpenes in turpentine capable of isomerization, and the absence of ethanol as a specific reaction medium can have a serious effect on the thermal isomerization process.

The sulfate turpentine used as the starting reactant in this study contained 75–80% α-pinene 1.2–1.5% camphene, 3–5% β-pinene, 11–14% 3-carene, 2–4% limonene, and other compounds. The sulfur content of sulfate turpentine was about 0.03–0.05%.

From both scientific and practical standpoints, it is pertinent to study the thermal isomerization of turpentine without a solvent, but under conditions similar to the α-pinene isomerization conditions in supercritical ethanol (comparable residence times, temperatures, and pressures). From the standpoint of science, it is interesting to compare the activation rate and rates of chemical reactions and to study the effect of pressure. For practical purposes, it is significant to estimate the yield of the desired products—limonene and alloocimenes—from turpentine isomerization without a solvent and to compare it to the yield of these products from α-pinene isomerization in supercritical ethanol under identical conditions. This comparison would be more correct and informative if the phase

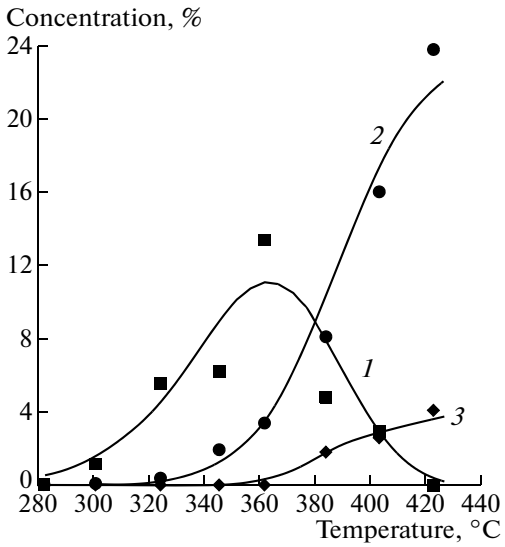

Fig. 11. Comparison between experimental and calculated data: (*1*) alloocimenes, (*2*) pyronenes, and (*3*) *p*-menthadienes. The lines represent the data calculated using the model, and the points represent experimental data.

compositions of turpentine and its thermolysis products under the experimental conditions were determined. To do this, it is necessary to know the critical parameters of the individual components of the multicomponent mixture of monoterpenes in sulfate turpentine and those of the anticipated thermolysis products. The necessary critical data were gained by calculations because no experimental data were available for most of the monoterpenes (Table 6). Table 6 lists the boiling points of some of the terpenes, which will be useful in the discussion of the results presented below.

The T_{cr} and P_{cr} values for limonene, 3-carene, alloocimenes, and some other monoterpenes (Table 6) were calculated using Joback's group contribution methods [67]. The results of these calculations demonstrate that the critical parameters of α-pinene and other monoterpenes that are either turpentine components or turpentine thermolysis products are similar: $T_{cr} \approx 615$–655 K and $P_{cr} \approx 24$–29 atm. Therefore, under the sulfate turpentine thermolysis conditions ($T = 533$–693 K, $P = 40$–280 atm; see Table 7), in the absence of any solvent, the reaction mixture can be either in the subcritical (liquid-like fluid) state or in the supercritical state, depending on the reaction temperature.

Main thermolysis products of sulfate turpentine. The most important experimental data for sulfate turpentine thermolysis at high pressures are presented in Table 7. These data were obtained from two series of experiments. In one of them, the thermolysis temperature was varied at a fixed pressure; in the other, the thermolysis pressure was varied at a constant temperature. The residence time of the reaction mixture in these two experimental series was the same. Most of the volatile products resulting from turpentine conversion were identified in each experiment. These products accounted for at least 94–95 wt % of the total product yield. A quantitative analysis of the reaction

Table 6. Calculated critical temperature, pressures, and molar volumes for some monoterpene hydrocarbons, water, and ethanol present in reaction mixtures in turpentine thermolysis in supercritical solvents

Component	T_{boil}, K (1 atm)	T_{cr}, K	P_{cr}, atm	V_{cr}, cm^3/mol
α-Pinene	445.9	632.5	28.9	484.5
β-Pinene	440.9	623.7	28.5	482.5
3-Carene	445.9	632.5	28.5	484.5
Limonen	448.6	646.0	27.6	496.5
β-Myrcene	425.7	615.2	23.9	539.5
4*E*,6*Z*-Alloocimene	440.6	642.8	24.7	537.5
4*E*,6*E*-Alloocimene	440.6	642.8	24.7	537.5
α-Pyronene	446.8	638.2	27.6	497.5
β-Pyronene	456.5	642.0	28.1	498.5
Silvestrene	448.7	646.0	27.2	496.5
α-Phellandrene	450.9	639.5	27.1	494.5
m-Mentha-1(6),4-diene	460.5	639.5	27.1	495.5
1,5,5-Trimethylcyclohepta-1,3-diene	455.8	654.8	29.0	490.5
Water	373.2	647.3	217.6	56.0
Ethanol	351.5	516.2	63.0	167.0

Table 7. Products resulting from the thermal isomerization of sulfate turpentine

			α-Pinene	Limonene	3-Carene	Alloocimenes	Pyronenes	Other products
Turpentine			80.0	1.3	11.0	0.0	0.0	7.7 (0.0)
entry	T, K	P, atm						
1	533	120	77.5	3.0	11.3	0.0	0.0	8.2 (0.6)
2	555		66.4	7.8	10.7	0.0	0.1	15.0 (8.8)
3	573		49.4	17.3	11.5	4.5	0.3	17.0 (9.8)
4	597		10.4	40.3	12.1	15.0	2.2	20.0 (12.1)
5	614		1.0	45.5	11.0	10.9	5.2	26.4 (18.1)
6	634		0.2	34.1	8.9	4.7	8.4	43.7 (36.2)
7	653		0.0	30.2	7.4	0.0	11.7	50.7 (42.6)
8	673		0.0	23.2	4.9	0.0	9.3	62.6 (50.5)
9	693		0.0	13.7	2.5	0.0	4.7	79.1 (60.1)
Turpentine			76.3	2.6	13.6	0.0	0.0	7.5
10	593	40	16.9	30.6	12.3	21.4	2.1	16.8
11		70	15.2	32.4	12.2	22.4	2.1	15.6
12		100	15.2	32.3	12.4	19.9	2.3	17.9
13		130	11.7	34.3	12.4	23.0	2.7	16.0
14		160	14.0	32.4	12.5	23.4	2.6	15.2
15		190	11.7	35.6	12.5	21.4	2.6	16.2
16		220	12.6	34.3	12.4	20.1	2.5	18.0
17		250	12.2	33.9	12.8	21.5	2.6	17.2
18		280	12.4	35.1	12.4	21.1	2.5	16.6

products demonstrated that the main thermolysis products of sulfate turpentine are limonene and alloocimene and pyronene isomers, as in the case of α-pinene thermolysis. Among the volatile compounds belonging to the group of "other products," we identified di- and monoalkylbenzenes (with methyl, ethyl, isopropyl, and isopropenyl substituents), trimethylcycloheptadienes, *p*- and *m*-trimethylcycloheptatrienes (terpinenes, terpinolene, phellandrenes), dimethyloctadienes (except alloocimenes), unreacted turpentine monoterpenes (camphene, fenchene, tricyclene), and C_{12}–C_{20} compounds.

The formation of each of the identified volatile products can be explained in the framework of the free-radical mechanisms of thermolysis of the corresponding monoterpenic hydrocarbons, such as the familiar free-radical mechanisms of the thermal isomerization of α- and β-pinene [41, 47], limonene [68], and 3-carene [69–72].

A comparison between the thermolysis of 3-carene—the second most abundant component of sulfate turpentine—alone in the gas phase at atmospheric pressure [70–72] and the thermolysis of 3-carene in turpentine reveals a difference between the conversion rates. In sulfate turpentine at $T = 673$ K ($\tau = 70$ s, $P = 120$ atm), the 3-carene conversion is over 50%, much higher than the conversion of pure 3-carene at $T = 753$ K ($\tau = 60$ s, $P \approx 1$ atm).

The percentages of nonvolatile reaction products included in the group of "other products" were estimated versus an internal standard (menthol) and were calculated as the difference between the total weight percent of volatiles in the initial sulfate turpentine and the total weight percent of the volatiles that remained in the reaction mixture after thermolysis. Since the amount of the gaseous products of pyrolysis in our experiments was small (as determined visually when sampling the products for analysis), we assumed that the decrease in the amount of volatile compounds in the reaction mixtures is due solely to the formation of oligomers that are nonvolatile under the GC-MS conditions. The thus-obtained quantitative data characterizing the component composition of the reaction mixtures seem to us quite reliable.

Note the following specific features of α-pinene conversion in supercritical ethanol (Fig. 2) and the conversion of α-pinene as a component of sulfate turpentine at 120 atm (Figs. 12, 13). Firstly, in α-pinene

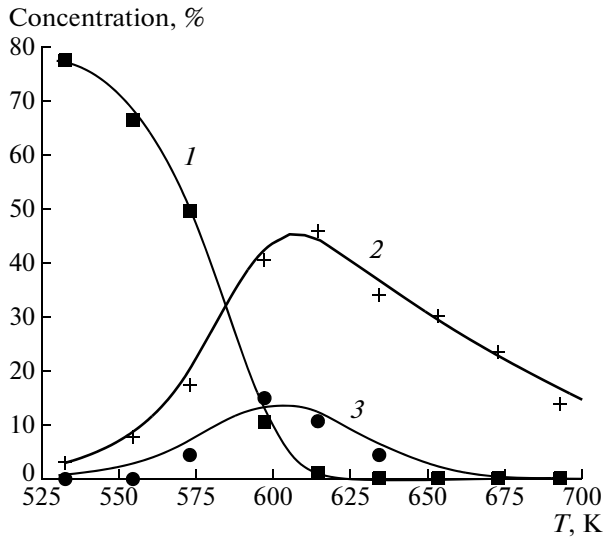

Fig. 12. Concentrations (mol %) of α-pinene as a turpentine component and its thermolysis products as a function of temperature (P = 120 atm, τ = 70 s): (*1*) α-pinene, (*2*) limonene, and (*3*) alloocimenes. The solid lines represent the data calculated using the model, and the points represent experimental data.

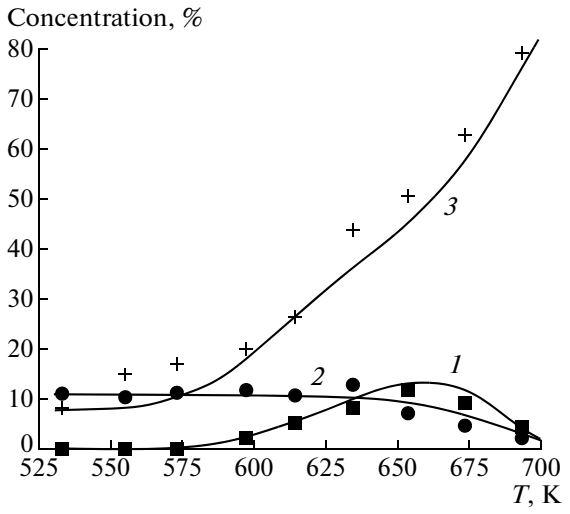

Fig. 13. Concentrations (mol %) of turpentine thermolysis products as a function of temperature (P = 120 atm, τ = 70 s): (*1*) pyronenes, (*2*) 3-carene, and (*3*) other products. The solid lines represent the data calculated using the kinetic model, and the points represent experimental data.

isomerization in supercritical ethanol, the limonene and alloocimene concentrations reach their maxima at complete α-pinene conversion; in the same process in turpentine, these concentrations reach their maxima at a lower α-pinene conversion of 90–92%. Secondly, while the concentration of pyronenes in α-pinene isomerization in supercritical ethanol increases steadily throughout the temperature range examined, the pyronene concentration in the thermolysis of sulfate turpentine passes through a maximum. Thirdly, the greatest difference between these reactions is in the formation rate of "other products," whose concentration increases sharply owing to the thermolysis of the products of α-pinene isomerization in turpentine.

This behavior of the reaction participants suggests that the monoterpenic compounds in supercritical ethanol are thermally more stable than the same compounds in the absence of a supercritical solvent. Note the low conversion of 3-carene and its insignificant contribution to the yield of "other products."

Another result of sulfate turpentine thermolysis that is in agreement with earlier data [34] is the formation of oligomers (>C_{25}–C_{30}) nonvolatile under the GC-MS conditions, whose amount can be up to 60 wt % of the total amount of thermolysis products (Table 7, entry 9).

Turpentine thermolysis kinetics. From the experimental data presented in Table 7, we derived a kinetic model for sulfate turpentine thermolysis. The reaction routes of this model are shown in Scheme 6.

Since the main component of sulfate turpentine is α-pinene, the reactions characteristic of individual α-pinene (reactions 1, 2, and 4 in Scheme 6) were used as the basis of the kinetic model. At the same time, the set of reactions included in Scheme 6 differs from that used in the kinetic model of α-pinene thermolysis in supercritical ethanol (Schemes 1, 2). Since the limonene and pyronene concentrations as a function of temperature pass through a maximum, the reactions limonene ⟶ "other products" (3), pyronene ⟶ "other products" (5), and 3-carene ⟶ "other products" (6) were included in the kinetic model for sulfate turpentine. Another distinction between this model and the model of α-pinene isomerization in supercritical ethanol is the absence of the alloocimenes ⟶ "other products" route in the former. This route was omitted for the reason that preliminary data processing based on identification of the complete kinetic model gave statistically unreliable values of the activation energy E and preexponential factor for the alloocimenes ⟶ "other products" reaction.

Experimental data with the above sulfate turpentine thermolysis reactions taken into account were processed using the plug-flow reactor model in the form of a set of ordinary differential equations with first-order rate equations for each route (Scheme 6). The calculated preexponential factors, activation energies, and their statistical characteristics are listed in Table 8. Figures 12 and 13 illustrate the good agreement between the experimental data (points) and the calculated data (lines). The only exception is the discrepancy between the experimental and theoretical temperature dependences of the "other products" concentration (Fig. 13). A possible cause of this discrepancy is disregard of the exact stoichiometry of reactions 3, 5, and 6 in Scheme 6.

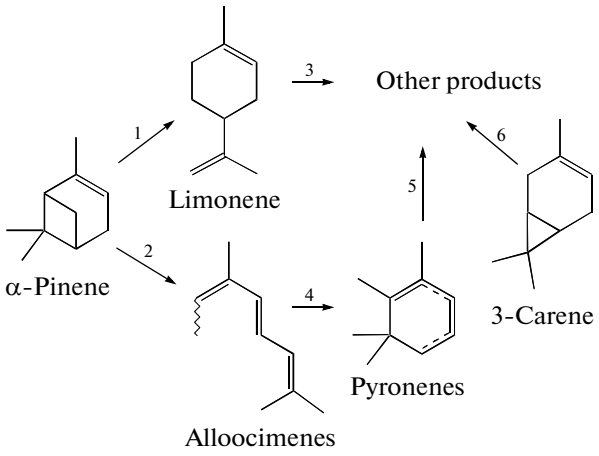

Scheme 6. Sulfate turpentine thermolysis routes.

Calculation of the overall reaction rate. To begin a comparison between the observed rates of α-pinene thermolysis in turpentine (Table 8) and the same data for α-pinene thermolysis in supercritical ethanol, it is necessary to find appropriate comparison parameters. The preferable ones are rate constants and activation energies. However, it would not be quite correct to directly compare k_0 and E for the same reactions, but in different kinetic models. For this reason, we introduce the concept of the overall rate of α-pinene conversion in turpentine, taking it to be the sum of the rates of the two main reactions, namely, α-pinene conversions into limonene and alloocimene isomers (reactions 1 and 2 in Scheme 6). For first-order reactions in a plug-flow reactor, the overall rate constant of α-pinene conversion in turpentine can be calculated via the equation

$$k_\Sigma(T,P) = \frac{\ln(y_0/y(T,P))}{\tau}, \quad k_\Sigma = k_1 + k_2, \qquad (23)$$

where y_0 and $y(T, P)$ are the α-pinene concentrations (mole fractions) in the feed and in the reaction product at a given temperature and pressure, respectively, and k_1 and k_2 are the rate constant of reactions 1 and 2 in Scheme 6 (Table 8).

The effect of the reaction medium temperature. Consider $\ln k_\Sigma$ as a function of $1000/T$ for the α-pinene conversions in turpentine (Fig. 14, curve *1*) and in supercritical ethanol (Fig. 14, curve *2*). At a given pressure, the overall rate constant of α-pinene conversion in turpentine is larger than the same rate constant in supercritical ethanol, and the activation energy E of the reaction in turpentine is higher than that of the reaction in supercritical ethanol:

In turpentine: $k_{\Sigma 0} = 2.69 \times 10^{11}$ 1/s,
$E = 149.4$ kJ/mol.

In supercritical ethanol: $k_{\Sigma 0} = 5.46 \times 10^{7}$ 1/s,
$E = 113.3$ kJ/mol.

Table 8. Estimates of kinetic constants and their statistical characteristics

Reaction	k_0, s^{-1}	E, kJ/mol
α-Pinene $\xrightarrow{1}$ limonene	$3.85 \times 10^{12} \pm 1.08 \times 10^{11}$	163.0 ± 4.11
α-Pinene $\xrightarrow{2}$ alloocimenes	$1.03 \times 10^{11} \pm 3.16 \times 10^{9}$	151.0 ± 4.59
Limonene $\xrightarrow{3}$ other products	$1.25 \times 10^{2} \pm 1.19 \times 10^{0}$	503.0 ± 1.54
Alloocimenes $\xrightarrow{4}$ pyronenes	$7.21 \times 10^{7} \pm 6.41 \times 10^{6}$	117.0 ± 13.9
Pyronenes $\xrightarrow{5}$ other products	$1.31 \times 10^{21} \pm 3.29 \times 10^{21}$	302.0 ± 430.0
3-Carene $\xrightarrow{6}$ other products	$1.15 \times 10^{14} \pm 3.34 \times 10^{13}$	209.0 ± 49.4

Standard deviation: 3.0%

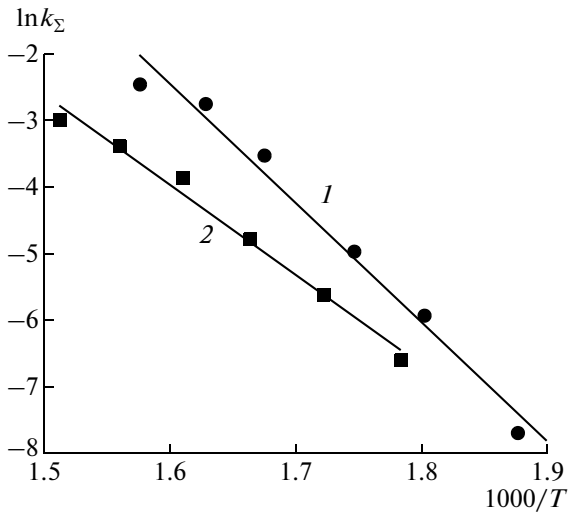

Fig. 14. Arrhenius plots of $\ln k_\Sigma$ versus $1000/T$: (*1*) turpentine and (*2*) supercritical ethanol. $P = 120$ atm; $\tau = 70$ s.

In order to explain this difference between the kinetic parameters of the reactions, we will find the activation parameters $\Delta\overline{H}^{\#}$, $\Delta\overline{S}^{\#}$, and $\Delta\overline{G}^{\#}$ of the α-pinene ⇄ [TS] reaction using transition state theory [73] and experimental values of the activation energy and rate constant $k_{\Sigma 0}$. The calculated values of the sought quantities, averaged over the temperature range of 533–693 K, are listed in Table 9.

Here, $\Delta\overline{H}^{\#}$ and $\Delta\overline{S}^{\#}$ have the meaning of the enthalpy of activation and entropy of activation averaged over the temperature range examined. Accordingly, $\Delta\overline{G}^{\#}$ is the averaged activation energy calculated as $\Delta G^{\#}(T) = \Delta\overline{H}^{\#} - T\Delta\overline{S}^{\#}$. It is clear from Table 9 that the entropy of activation is negative for both systems, implying that the [TS] structure is more ordered than the structure of the initial α-pinene molecule. This ordering is likely due to the loss of the rotational degree of freedom by one CH_3 group or more. The absolute value of the entropy of activation of [TS] in supercritical ethanol is much higher than the $\Delta\overline{S}^{\#}$ of [TS] in turpentine. This possibly means that [TS] is more ordered in supercritical ethanol, in which the α-pinene concentration was 50 times lower than in turpentine. Unfortunately, the available data are insufficient to make certain whether the [TS] ordering is due to the lower initial α-pinene concentration or the solvent effect.

Despite the marked differences in $\Delta\overline{H}^{\#}$ and $\Delta\overline{S}^{\#}$, the temperature-averaged values of $\Delta\overline{G}^{\#}$ for the reactions of α-pinene in turpentine and in supercritical ethanol are similar. This fact may indicate that the thermolysis mechanism (and [TS] structure) of α-pinene changes only slightly on passing from one reaction medium to another. Using the familiar thermodynamic relationship between the equilibrium constant $K_{eq}^{\#}$ and the Gibbs energy of a reaction,

$$K_{eq}^{\#} = \exp\left(-\frac{\Delta G^{\#}(T)}{RT}\right), \qquad (24)$$

it can be demonstrated that, for the α-pinene ⇄ [TS] reaction, the $K_{eq}^{\#}(T)$ values for the turpentine medium are larger than those for supercritical ethanol (Fig. 15). The larger value of the equilibrium constant $K_{eq}^{\#}$ means that the equilibrium [TS] concentration in turpentine is higher than that in supercritical ethanol, and this may be responsible for the higher overall α-pinene conversion rate in turpentine.

Heat-Induced Conversions of cis-Verbenol in Supercritical Ethanol

A comparison between the reactivities of α- and β-pinene in their thermal isomerization reactions, measurement of reaction rates, and determination of the corresponding activation energies would make it possible to establish a correlation between the structure and chemical properties of these structurally similar compounds. Additional information for establishing this structure–properties correlation can be gained by investigating the thermal isomerization of related compounds having the same carbon backbone, but different functional groups. One of the pinene relatives is *cis*-verbenol, derivative having an OH group in the allyl position at the C-4 atom. This OH group is *cis* to the gem-dimethyl fragment of cyclobutane. It is,

Table 9. Mean values of the activation parameters of the transition state

System	$\Delta\overline{H}^{\#}$, kJ/mol	$\Delta\overline{S}^{\#}$, J/(mol K)	$\Delta\overline{G}^{\#*}$, kJ/mol
α-Pinene in turpentine	144.4	−40.3	169.0 (165.4–172.6)
α-Pinene in supercritical ethanol	116.9	−96.2	175.6 (166.9–184.3)

Note: $T = 533$–693 K, $P = 120$ atm, $\tau = 70$ s.

* The numbers in parentheses are the minimum and maximum values.

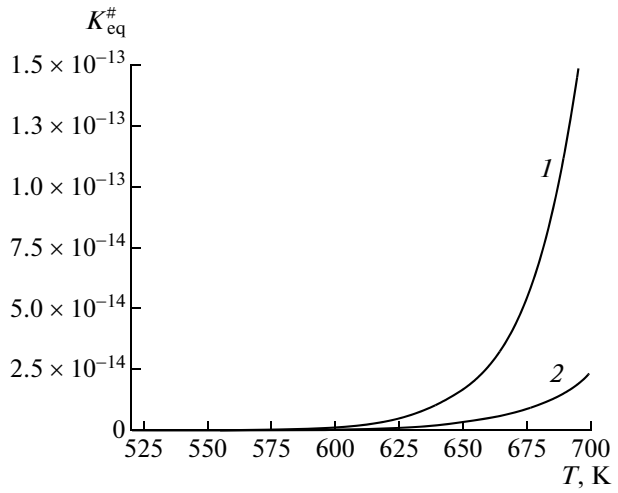

Fig. 15. Equilibrium constant $K_{eq}^{\#}$ as a function of temperature: (*1*) turpentine and (*2*) supercritical ethanol. $P = 120$ atm; $\tau = 70$ s.

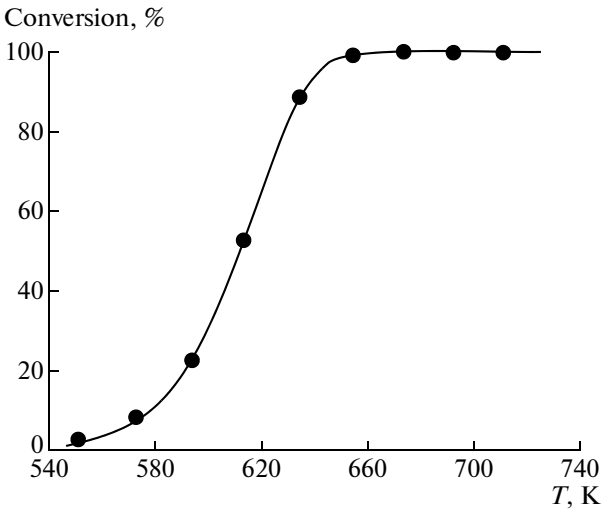

Fig. 16. *cis*-Verbenol conversion as a function of temperature. $P = 120$ atm; $\tau = 70$ s. The points represent experimental data, and the solid line is the result of data processing.

therefore, interesting to study and understand the effect of this heterofunctionality on the conversion routes and thermal isomerization energetics of *cis*-verbenol.

There have been only a few studies of the thermal isomerization of *cis*-verbenol in the gas and liquid phases [3, 4, 74]. According to these studies, the main products of this reaction are isopiperitenol (no information about whether *cis* or *trans*) and *cis*/*trans*-citral isomers, which likely result from the successive opening of the four- and six-membered rings of the bicyclic pinane structure. It was noted that small amounts of heavy and light hydrocarbons were present in the reaction mixture.

For further investigation of the reactions of terpenes in supercritical solvents, the thermal isomerization of verbenol was carried out in supercritical ethanol at various temperatures and a constant pressure. As a result, we determined the verbenol conversion as a function of the reaction temperature (Fig. 16). The identified initial compounds and reaction products are listed in Table 10. Analysis demonstrated that the initial verbenol contained 92.6% *cis*-verbenol, 4.7% *trans*-verbenol, about 1.4% verbenene, and 0.4% verbenone. *cis*-Citral, *trans*-citral, and isogeranial were reliably identified in the reaction products, and this confirmed the results of an earlier [74]. According to that work, the main verbenol isomerization product is isopiperitenol, whose amount is 60–70 vol %. Unfortunately, Maksimchuk et al. [74] did not identify the piperitenol isomers (*trans*- and *cis*-isopiperitenol) and referred to them as a single compound—isopiperitenol. In the studies reported here, the unavailability of pure *cis*- and *trans*-isopiperitenols and piperitenol and lack of the corresponding retention index data did not allow us to reliably identify these compounds in the product mixture. However, the GC data for *trans*-isopiperitenol available from an earlier publication [75] and the chromatograms and mass spectra of *trans*-isopiperitenol kindly presented on our request by Rodney Croteau, one of the authors of this publication, enabled us to identify this compound among the products of verbenol isomerization in supercritical ethanol. In Table 11, the mole fraction of *trans*-isopiperitenol and the sum of the mole fractions of *cis*-isopiperitenol and piperitenol are presented in separate rows.

Experimental data demonstrate that conducting *cis*/*trans*-verbenol isomerization in supercritical ethanol affords a significant increase in the reaction rate and ensures almost complete *cis*/*trans*-verbenol conversion at a comparatively low temperature of 380°C (in gas-phase isomerization, no noticeable verbenol conversion is observed at this temperature [74]). The yield (selectivity) of the desired product—*cis*- and *trans*-citrals—increases from 8% in the gas phase [74] to 38% in supercritical ethanol.

Note the temperature dependence of the mole fractions of reactants (Table 10). On the one hand, the complete *cis*- or *trans*-verbenol conversion point coincides with the *cis*- and *trans*-citral peak; on the other hand, it is accompanied by the formation of large amounts of light an heavy hydrocarbons, which likely result from the pyrolysis of the citrals, *trans*- and *cis*-isopiperitenols, and piperitenol. It is, therefore, difficult to explain why the concentrations of *trans*- and *cis*-isopiperitenols and piperitenol begin to decrease when verbenol is still present in the reaction mixture. For this reason, we had to augment the reaction net-

Table 10. Experimental data on the thermal isomerization of verbenol in supercritical ethanol

Entry	Compound	Temperature, °C								
		278	300	321	340	361	381	400	419	438
1	*cis*-Verbenol	93.45	88.02	74.72	45.62	10.61	0.83	0.00	0.00	0.00
2	*trans*-Verbenol	3.79	3.41	2.69	1.35	0.70	0.16	0.00	0.00	0.00
3	Neral (*cis*-citral)	0.40	1.63	4.58	10.43	15.61	16.12	15.24	11.83	5.64
4	Geranial (*trans*-citral)	0.07	0.57	2.08	7.05	16.21	20.12	19.61	15.36	7.74
5	Isogeranial	0.12	0.70	2.16	4.72	7.24	7.51	7.88	6.42	3.42
6	Isocyclocitral	0.00	0.25	0.97	2.87	5.31	6.19	6.53	6.40	6.36
7	*trans*-Isopiperitenol	0.83	2.37	5.84	12.17	16.33	11.85	7.64	4.87	1.44
8	*cis*-Isopiperitenol and piperitenol	0.34	1.09	2.77	5.68	6.75	4.01	2.96	2.11	1.53
9	Other compounds	1.00	1.96	4.19	10.11	20.86	27.75	33.49	40.85	36.58
10	Resins and nonvolatile components	0.00	0.00	0.00	0.00	0.38	5.46	6.65	12.16	37.29

Table 11. Compositions of azeotropic mixtures at various pressures (initial mixture composition, mol %: α-pinene, 10; ethanol, 10; water, 80)

P_{az}, atm	T_{az}, K	Liquid 1		Liquid 2		Vapor	
		α-pinene	ethanol	α-pinene	ethanol	α-pinene	ethanol
1	352.4	0.00	0.53	45.23	43.37	5.05	54.34
5	402.8	0.00	1.19	40.39	36.79	5.49	43.58
10	430.6	0.00	1.62	36.53	32.24	5.84	37.36
20	463.2	0.00	2.11	30.87	26.47	6.30	30.23
40	502.0	0.02	2.55	22.80	19.55	6.81	22.32
60	528.0	0.07	2.73	17.08	15.19	7.02	17.51
80	548.4	0.18	2.82	12.80	12.04	6.99	14.01

work with the conversion of *trans*- and *cis*-isopiperitenols, and piperitenol into "other products":

1. *cis*-Verbenol ⟶ *cis*-citral.
2. *cis*-Verbenol ⟶ *trans*-isopiperitenol.
3. *cis*-Verbenol ⟶ *cis*-isopiperitenol + piperitenol.
4. *cis*-Verbenol ⟶ isogeranial.
5. *cis*-Citral ⟶ "other products."
6. *cis*/*trans*-Isopiperitenol + piperitenol ⟶ "other products."

The apparent overall activation energy determined by Maksimchuk et al. [74], 96.7 kJ/mol, differs greatly from the value obtained in this study, 157 kJ/mol.

As follows from the results of this work, the activation energy of thermal isomerization of monoterpenic compounds (such as β-pinene; see Scheme 4) in supercritical alcohols is also higher than the activation energy of thermal isomerization of these compounds in the gas or liquid phase at atmospheric pressure. A possible cause of this significant difference is that the supercritical solvent changes the properties of the activated complex and thus shifts the equilibrium in the reversible step of the reaction toward the final product.

EFFECT OF PRESSURE ON THE RATE OF THERMAL ISOMERIZATION OF MONOTERPENIC COMPOUNDS IN SUPERCRITICAL ALCOHOLS

A specific feature of many organic reactions n supercritical fluids is that their rate or rate constant depends strongly on pressure [37, 76–78]. The effect of pressure on the rate constant is typical of reactions in aqueous solutions. For reactions in supercritical solvents, an increase in pressure (density of the medium) can lead both to an increase in the reaction rate [37, 79–84] and to a slowdown of the reaction [79, 85–88] or cause the reaction rate to pass through an extremum [79, 89]. In any case, the effect of pressure on the rate constant can be explained in terms of the

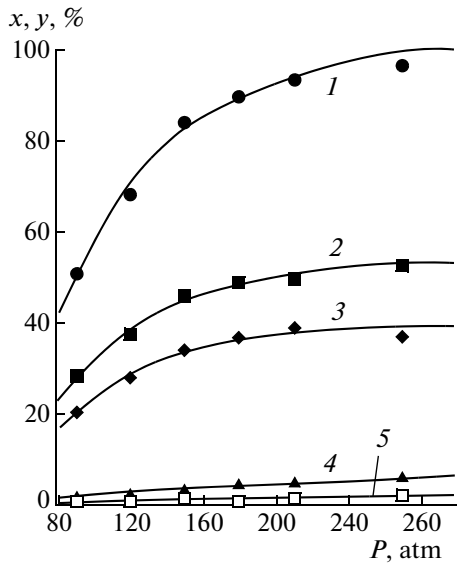

Fig. 17. α-Pinene conversion (x) and the yield of isomerization products (y) as a function of pressure: a comparison between experimental data (points) and calculated data (lines). $T = 600$ K; $\tau = 70$ s.

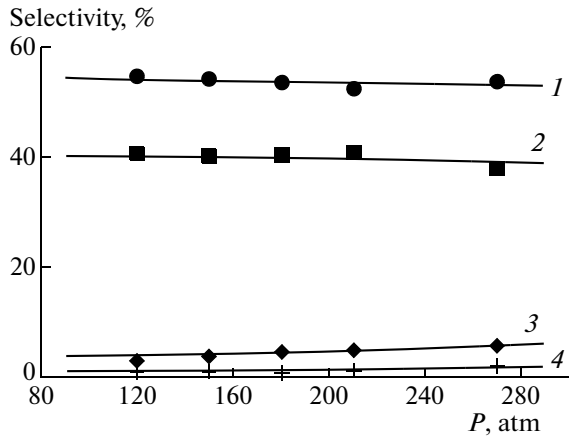

Fig. 18. Product selectivities of the reaction as a function of pressure: (*1*) limonene, (*2*) alloocimene isomers, (*3*) pyronene isomers, and (*4*) other products. $T = 600$ K; $\tau = 70$ s. The points represent experimental data, and the lines represent calculated data.

specific interaction of the solvent with the solute molecules, the properties and nature of the supercritical solvent, or the interaction of the solute molecules or clusters with the solvent.

Experiments on the thermal isomerization of α-pinene in supercritical ethanol also demonstrated that the pressure of the reaction medium exerts a significant effect on the rate of parallel reactions of α-pinene (Fig. 17). At the same time, pressure variation does not produce any appreciable effect on the selectivity of the reaction (Fig. 18).

The effect of the solvent pressure (density) on the apparent rate constants of thermal α-pinene isomerization was explained and quantitatively described using transition state theory [73]. According to this theory, as the reaction moves along the reaction coordinate, it surmounts a potential energy barrier, whose peak corresponds to the maximum potential energy of the activated complex, or the transition state [TS] between the molecule of reactant A and the molecule of product B (for monomolecular reactions): A $\rightleftharpoons$ [TS] $\rightleftharpoons$ B. Here, the [TS] formation step is reversible and is the most rapid in the overall reaction A $\longrightarrow$ B. Applying the postulates of transition state theory to the thermal isomerization of α-pinene (Scheme 2), we can represent this process as the following two reactions: α-pinene $\rightleftharpoons$ $[TS]_1 \longrightarrow$ limonene (route 1) and α-pinene $\rightleftharpoons$ $[TS]_2 \longrightarrow$ alloocimenes (route 2). The introduction of two structurally different activated complexes, $[TS]_1 \neq [TS]_2$, is quite appropriate because of the formation of two different isomers via two parallel reactions and because the activation energies of these reactions differ by ~19 kJ/mol (Table 2).

The reaction rates as a function of pressure for routes 1 and 2 at a constant experimental temperature of $T_0 = 600$ K are written as

$$R_1(T_0,P) = k_1(T_0,P)y^{\#} \quad R_2(T_0,P) = k_2(T_0,P)y^{\#}, \quad (25)$$

where $y^{\#}$ is the dimensionless equilibrium concentration of $[TS]_i$; $i = 1, 2$.

The pressure dependence of the apparent rate constants can be expressed as the following equation [90]:

$$\frac{\partial}{\partial P}\left(\ln\frac{k_{i,\mathrm{app}}(T_0,P)}{k_i(T_0,P_0)}\right) = \frac{1}{RT}\left(\frac{\partial \ln \Phi_{A_1}}{\partial P} - \frac{\partial \ln \Phi_{TS}}{\partial P}\right) = \frac{-\Delta \bar{V}^{\#}}{RT}, \quad i = 1,2, \quad (26)$$

where $k_{i,\mathrm{app}}$ is the apparent rate constant of route 1 or 2. The numerical values of $k_1(T_0,P_0)$ and $k_2(T_0,P_0)$ ($T_0 = 600$ K, $P_0 = 120$ atm) are derived from the above experimental data (Table 1).

The fugacity coefficients $\Phi_i = \Phi_i(\mathbf{y},T,P)$ in Eq. (26) are functions of temperature, pressure, critical parameters and other properties of the individual components, and the molar composition of the mixture. The numerical value of the volume of activation (which is equal to the difference between the partial molar volumes of the activated complex and the reactant, $\Delta \bar{V}^{\#} = \bar{V}_{\mathrm{TS}} - \bar{V}_{\mathrm{A}}$) depends on the internal properties of the system, on the properties of the reactant, and on the external factors determined by the solvent. The $\Delta \bar{V}^{\#}$ value can be both positive and negative.

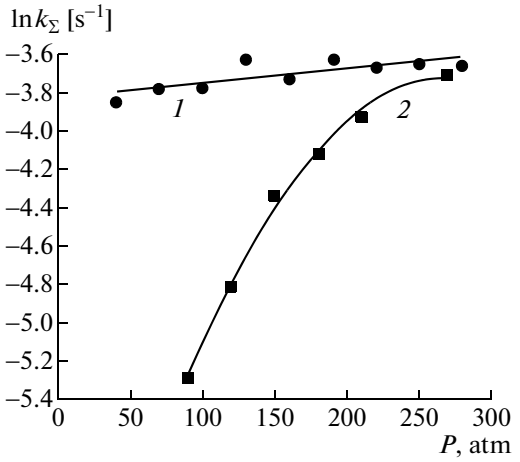

Fig. 19. lnk_Σ versus pressure: (*1*) turpentine ($T = 593$ K) and (*2*) supercritical ethanol ($T = 600$ K).

Integration of Eq. (26) between P_0 and P (P_0 = 120 atm) yields the apparent rate constants as a function of pressure in the following form:

$$\ln k_{i,\text{app}}(T_0,P) = \ln k_i(T_0,P_0) - \frac{1}{RT}\int_{P_0}^{P}\Delta\bar{V}^{\#}(P)\,\mathrm{d}P \quad i = 1,2. \tag{27}$$

Solving the parameter identification problem using a pressure-dependent data array. Sine there is no explicit $\Delta\bar{V}^{\#}(P)$ relationship, it seems impossible to use Eq. (27) in the determination of the apparent rate constants. The problem can be solved by using the mean-value theorem, dividing the continuous integration interval in Eq. (27) into discrete intervals P_1–P_0, P_2–P_0, ..., P_k–P_0 and replacing $\Delta\bar{V}^{\#}(P)$ with the mean integral values $\Delta\tilde{V}_k^{\#}$ in the P_k–P_0. intervals. This will bring Eq. (27) to the following form:

$$\ln k_{i,\text{app}}(T_0,P_k) = \ln k_i(T_0,P_0) - \frac{\Delta\tilde{V}_k^{\#}}{RT}\int_{P_0}^{P_k}dP = \ln k_i(T_0,P_0) - \frac{\Delta\tilde{V}_k^{\#}}{RT}(P_k - P_0). \tag{28}$$

The mean integral value $\Delta\tilde{V}_k^{\#}$ in the kth interval remains a function of pressure, so the dependence of $\Delta\tilde{V}_k^{\#}$ on P in each interval is representable as a quadratic polynomial,

$$\Delta\tilde{V}_k^{\#} = b_0 + b_1P + b_2P^2, \tag{29}$$

in which the coefficients b_1, b_2, and b_3 are the unknown parameters of the model. To determine these coefficients, we solved the inverse problem for the reaction routes presented in Scheme 2 by minimizing the objective function (4) and calculated the component concentrations by numerically integrating the set of equations (3). The apparent rate constants in Eq. (3) are now functions of pressure:

$$k_{i,\text{app}} = k_i(T_0,P_0)\exp\left(-\frac{\Delta\tilde{V}^{\#}(P)}{RT}(P - P_0)\right). \tag{30}$$

Solving the inverse problem yielded the following values of the sought coefficients of expression (29):

$$b_0 = -1974.63 \pm 136.85, \quad b_1 = 13.15 \pm 0.91,$$
$$b_2 = -0.022 \pm 0.002.$$

It is clear from experimental data (Fig. 17) that pressure has a significant effect only on the rate constants of routes 1 and 2 in Scheme 2, raising the yields of limonene and alloocimenes. Although the yields of pyronenes and "other products" are seemingly pressure-independent, the pressure-induced increase in the concentration of alloocimenes—precursors of pyronenes and "other products"—must certainly change the concentrations of the latter.

The calculated $\Delta\tilde{V}^{\#}$ values are negative over the pressure range examined; therefore, the rate constants grow with increasing pressure. The most rapid increase of the constants is observed in the 90–120 atm range, in the nearest vicinity of the critical pressure of the solvent (ethanol).

The model suggested here is in good agreement with the experimental data indicating the constancy of the α-pinene isomerization selectivity (Fig. 18). This follows immediately from the model because the pressure-induced increase in the rate constants of the reactions in the α-pinene ⟶ limonene and α-pinene ⟶ alloocimenes routes does not change the rate constant ratio $k_1(T,P)/k_2(T,P)$, the quantity determining the selectivity of the reaction.

Effect of Pressure on the Turpentine Isomerization Rate

Above, we discussed the reactions of α-pinene in sulfate turpentine at a constant pressure of 120 atm and variable temperature (based on the experimental data presented in Table 7), compared them with the reactions of α-pinene in supercritical ethanol, suggested a kinetic model, and determined its parameters. Here we will process the experimental data presented in Table 7 to elucidate the effect of pressure on the rate and selectivity of thermolysis of α-pinene as a component of sulfate turpentine. For this purpose, we will again use the overall rate constant of α-pinene conversion (k_Σ) in turpentine calculated via Eq. (23) for the data listed in the second part of Table 7.

Figure 19 plots the ln k_Σ versus pressure dependence derived from experimental data for α-pinene thermolysis in turpentine along with the same dependence for α-pinene isomerization in supercritical ethanol. The fact that the rate constant of α-pinene isomerization in supercritical ethanol increases with increasing pressure was explained in terms of transi-

tion state theory, in which the pressure dependence of the rate constant is determined by the sign of the volume of activation, $\Delta V^{\#}$, according to Eq. (26).

Experimental pressure-dependent $\ln \ln k_\Sigma$ data allow the $\Delta V^{\#}$ value to be determined using Eq. (26). Since the dependence of $\ln \ln k_\Sigma$ on P for the reaction of α-pinene in turpentine (Fig. 19) is linear, the $\Delta V^{\#}$ value of this reaction is pressure-independent. In this case, integration of Eq. (26) in which $k_{i,\text{app}}$ is replaced with k_Σ yields the expression

$$\ln k_\Sigma = \ln k_0 - \frac{\Delta V^{\#}}{RT} P, \quad (31)$$

where $\ln k_0$ is the rate constant at $P = 0$.

The pressure dependence of $\ln k_\Sigma$ for α-pinene isomerization in supercritical ethanol (Fig. 19) is nonlinear, clearly indicating that the $\Delta V^{\#}$ value of this reaction is pressure-dependent. The linear fit for experimental data for α-pinene in turpentine,

$$\ln k_\Sigma = -3.8305 + 0.000758P, \quad (32)$$

and the polynomial fit for α-pinene in supercritical ethanol,

$$\ln k_\Sigma = -7.2495 + 0.02632P - 4.919 \times 10^{-5} P^2 \quad (33)$$

make it possible to calculate the corresponding $\Delta V^{\#}$ values via Eq. (31). For α-pinene thermolysis in turpentine, Eqs. (31) and (32) lead to $\Delta V^{\#} = -37$ cm^3/mol. For α-pinene in supercritical ethanol, $\Delta V^{\#}$ is also negative and depends linearly on pressure, varying between −858 and −36 cm^3/mol in the pressure range of 90–270 atm. It is this variation of the volume of activation that causes the reaction rate to increase with increasing pressure.

The difference between the α-pinene isomerization rates in turpentine and supercritical ethanol is clearly illustrated by the dependence of $\ln k_\Sigma$ on the density of the medium (Fig. 20). The latter was calculated using the Peng–Robinson equation [91]. It follows from Fig. 19 that the density of α-pinene as a component of turpentine is higher than the density of α-pinene in supercritical ethanol throughout the pressure range and varies insignificantly with pressure.

No chemical reaction can be examined separately from the medium in which it occurs. For many reactions in gaseous and liquid solvents and supercritical media, it is to be expected that, as the pressure is raised, the reaction rate and the position of the equilibrium will alter because of the changes in the character and intensity of intermolecular interactions between the solute and the solvent. Depending on the properties of the solvent and solute, an increase in the solvent pressure or density can increase the solvation number, the frequency of molecular collisions, and the

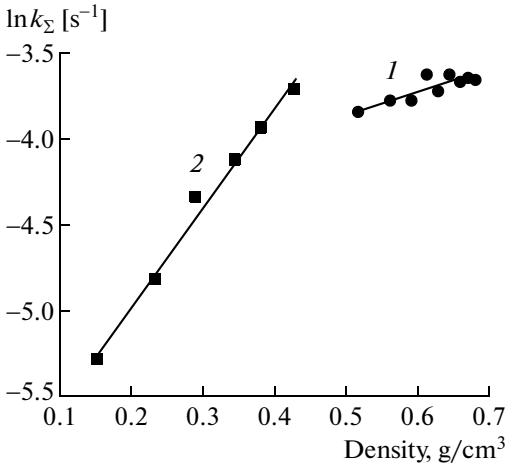

Fig. 20. $\ln k_\Sigma$ as a function of the density of the solution: (*1*) turpentine ($T = 593$ K) and (*2*) supercritical ethanol ($T = 600$ K).

[TS] concentration, and this will inevitably accelerate the reaction. If the density stops growing as the pressure is further raised, as in the case of supercritical fluids in the critical region, the pressure effect on the rate constant will decrease.

Effect of Pressure on the α-Pinene Isomerization Rate in Water-Containing Supercritical Ethanol: The Ionic Mechanism of the Reaction

As was demonstrated above, the water ionic product K_w increases in proportion to water density, according to relationship (7), bringing about an increase in the H^+ concentration. This causes an increase in the reaction rate. An increase in pressure in the supercritical ethanol + water + α-pinene system leads to an increase in the density of the supercritical medium according to its equation of state and, accordingly, to an increase in the ion concentration. Although ethanol contains only 4–5% water, the pressure-induced increase in the H^+ concentration speeds up the reaction via the ionic mechanism of α-pinene isomerization, as follows from Eq. (16).

THERMODYNAMICS OF MONOTERPENE MIXTURES IN SOLVENTS

The α-pinene–water and α-pinene–ethanol–water systems under normal conditions belong to the class of immiscible or separating liquids. There are no experimental data concerning phase equilibria in these systems at high temperatures and pressures up to the critical region. At the same time, kinetic and mechanistic studies of monoterpene isomerization in supercritical solvents need knowledge of critical parameters and the way they vary with the composition of the reaction mixture. This is the reason why we used thermodynamic simulation as the main tool in our study of

the phase state of two- and three-component systems and in the calculation of critical parameters.

Equation of state. Under subcritical and supercritical conditions, the reaction system cannot be described in terms of ideal gas or ideal solution laws, which assume that the mixture components are energetically independent. In view of this, the state of reaction mixtures is calculated using two-parameter cubic equations of state, such as the Redlich–Kwong–Soave, Peng–Robinson, and Patel–Teja equations. In our study, the phase states and the thermodynamic and thermophysical properties of multicomponent mixtures were calculated using the Redlich–Kwong–Soave (RKS) equation of state [91]:

$$P = \frac{RT}{V_m - b_m} - \frac{a_m(T)}{V_m(V_m + b_m)}, \quad (34)$$

where V_m is the molar volume of the mixture (l/(g mol)). The coefficients a_m and b_m for a mixture with a given molar composition vector **y** are defined as follows:

$$a_m = \sum_{j=1}^{N_s}\sum_{i=1}^{N_s} y_i y_j a_{ij}, \quad b_m = \sum_{j=1}^{N_s}\sum_{i=1}^{N_s} y_i y_j b_{ij}, \quad (35)$$

$$a_{ii} = \alpha_i(T)\left(0.42748R^2T_{i,\mathrm{cr}}^2/P_{i,\mathrm{cr}}\right), \quad b_{ii} = 0.08664RT_{i,\mathrm{cr}}/P_{i,\mathrm{cr}}, \quad (36)$$

$$a_{ij} = (1-k_{ij})\sqrt{a_{ii}a_{jj}}, \quad b_{ij} = (1-c_{ij})(b_{ii}+b_{jj})/2, \quad (37)$$

$$\alpha_i(T) = \left[1 + d_i\left(1 - \sqrt{T/T_{i,\mathrm{cr}}}\right)\right]^2, \quad d_i = 0.480 + 1.574\omega_i - 0.176\omega_i^2.$$

Here, $T_{i,\mathrm{cr}}$ and $P_{i,\mathrm{cr}}$ are, respectively, the critical temperature and critical pressure of the ith component of the mixture. The parameter ω_i, called the acentric factor, can be found in thermochemical handbooks, and k_{ij} and c_{ij} are binary interaction coefficients. The accuracy of the calculation of the phase diagrams and critical parameters of complex depends strongly on whether k_{ij} and c_{ij} in Eq. (37) are correctly chosen or calculated using experimental data available on binary equilibria. In view of this, we earlier suggested a k_{ij} and c_{ij} determination procedure [92] taking into account the temperature and pressure dependences of these coefficients. When there were no necessary experimental data, the binary interaction coefficients were taken to be zero in most cases.

Calculating the Critical Point for a Multicomponent Mixture of a Given Composition

A mixture of a given composition is in the critical state when its temperature $T_{\mathrm{mix,cr}}$ and pressure $P_{\mathrm{mix,cr}}$ are such that the following conditions are satisfied simultaneously [93, 94]:

$$F_1(T,P) \equiv \mathrm{Det}(\mathbf{M}_1) = 0, \quad (38)$$

$$F_2(T,P) \equiv \mathrm{Det}(\mathbf{M}_2) = 0. \quad (39)$$

The elements of the matrix $\mathbf{M}_1$ in Eq. (38) are the first derivatives of the natural logarithms of the fugacities of components with respect to the umber of their moles calculated at a constant pressure and temperature:

$$\mathbf{M}_1 = \left\{\frac{\partial \ln f_i}{\partial n_j}\right\}_{T,P} \quad i = 1, 2, \ldots, N;\ j = 1, 2, \ldots, N, \quad (40)$$

where N is the number of components in the mixture.

The fugacity of the components, $f_i(T,P,\mathbf{y})$, which is a function of temperature, pressure, and the molar composition of the mixture (vector **y**), is conventionally calculated using cubic equations of state.

The matrix $\mathbf{M}_2$ in Eq. (39) is obtained from the matrix $\mathbf{M}_1$ by replacing any of its rows with the row vector

$$[\partial F_1/\partial n_1, \partial F_1/\partial n_2, \ldots, \partial F_1/\partial n_N]. \quad (41)$$

Equation (38) defines a spinodal line (sp) in the T–P plane. It is monovariant and, for any mixture composition, has a set of solutions in terms of the interdependent pair of values $T_{\mathrm{sp}}(P_{\mathrm{sp}})$ to $P_{\mathrm{sp}}(T_{\mathrm{sp}})$ satisfying Eq. (38). The criterion of spinodal stability (StCrit) or spinodal instability of a mixture of a given composition is the value of function (38) at an arbitrary temperature and pressure. If StCrit < 0, the mixture is considered to be spinodally stable. Conversely, if StCrit > 0, the mixture is considered to be spinodally unstable.

The critical point of a mixture, ($T_{\mathrm{mix,cr}}$, $P_{\mathrm{mix,cr}}$), is a singular point in the spinodal curve, simultaneously satisfying Eqs. (38) and (39).

For solving the above mathematical problem, we suggested an equivalent form of the critical phase equations (38) and (39) [95], which substantially simplified numerical calculations. The problem was solved by the homotopy method.

Model for Calculating Gas–Liquid, Liquid–Liquid, and Gas–Liquid–Liquid Phase Boundaries

In the calculation of the phase boundaries separating homogeneous fields, gas–liquid and liquid–liquid two-phase fields, and gas–liquid–liquid three-phase fields, we used familiar thermodynamic models of monovariant binodal lines [96], also known as tangent plane equations [97]. In the general case, at a fixed composition of one of the phases, each temperature and pressure make a pair of interdependent values minimizing the function

$$F(\mathbf{x},T,P) \equiv \frac{\Delta G}{\varepsilon RT} = \frac{1}{RT}\sum_{i=1}^{N} x_i[\ln x_i + \ln\Phi_i(x,T,P) - \ln z - \ln\Phi_i(\mathbf{z},T,P)] \to \min \quad (42)$$

under the constraint

$$\sum_{i=1}^{N} x_i = 1, \quad (43)$$

where $\Delta \boldsymbol{G}$ is the Gibbs energy of phase transition, $\mathbf{x}$ is the vector of mole fractions of the components forming in infinitely small amounts (ε) in the new equilibrium phase, $\mathbf{z}$ is the vector of the mole fractions of the components in the initial mixture of a given composition, and $\Phi_i(\mathbf{x},T,P)$ and $\Phi_i(\mathbf{z},T,P)$ are the corresponding fugacity coefficients calculated using an equation of state. Equation (42) subject to constraint (43) is monovariant: at a given $\mathbf{z}$, there are only interdependent $T_b(P_b)$ or $P_b(T_b)$ pairs satisfying Eqs. (42) and (43). Obviously, the following condition should be satisfied at the minimum points of Eq. (42):

$$\det[\mathbf{h}_x] > 0 \quad \det[\mathbf{h}_z] > 0, \quad (44)$$

where $\mathbf{h}_x$ and $\mathbf{h}_z$ are symmetrical matrices with the elements

$$\mathbf{h}_x = \left\{\frac{\partial^2 F}{\partial x_i \partial x_j}\right\}, \quad \mathbf{h}_z = \left\{\frac{\partial^2 F}{\partial z_i \partial z_j}\right\}, \quad (45)$$
$$i = 1,2,\ldots,N, \quad j = 1,2,\ldots,N.$$

In the case of a system having three equilibrium phases, e.g., a gas phase and two immiscible liquid phases, the properties of the vapor can be derived from the properties of any of the two liquid phases using the phase equilibrium condition for this system:

$$f_i^{(l_1)} = f_i^{(l_2)} = f_i^{(v)}. \quad (46)$$

To do this, it is necessary to calculate the equilibrium between the two liquid phases at a given overall composition of the heterogeneous liquid mixture. Division into two liquid phases is done by a standard flash method [98]. Next, using models (42) at a fixed pressure and a fixed composition of the liquid phase (in our case, the α-pinene-rich phase), the vapor composition and temperature satisfying conditions (42) and (43) are calculated.

Calculation Results and Discussion

α-Pinene–water system. Two-component liquid–liquid–vapor systems have one degree of freedom. This means that a separating heterogeneous mixture at a fixed pressure will evaporate at a constant temperature and the composition of its phases will not change until one of the liquid phases disappears. Such systems are called heteroazeotropic [91, 97], with coordinates T_{az} and P_{az}, where P_{az} is the vapor pressure over the immiscible liquids, which is equal to the total pressure, and T_{az} is the boiling temperature of the azeotropic mixture.

The α-pinene–water binary system is a heteroazeotropic system because α-pinene and water are practically immiscible under normal conditions. If the temperature and pressure increase, the liquid phases will dissolve in one another and their components will pass into the vapor phase. Once the critical parameters have been reached, the two-phase system will become a homogeneous system.

The above models are quite appropriate for calculating the phase states of reaction mixtures containing α-pinene, water, and α-pinene thermolysis products, such as limonene, alloocimenes, and pyronenes. The phase diagrams of systems containing these reaction products will be very similar, both quantitatively and qualitatively, to the diagrams calculated for the α-pinene–water system. This is confirmed by the critical parameters of α-pinene and some other monoterpenes calculated from structural data using group contribution methods [67].

Figure 21 presents the calculated phase diagrams of the binary mixture at 20 and 50 atm. Either diagram has five characteristic fields: **L–L**, **L–V$_1$**, **L–V$_2$**, **Liq**, and **Vap**. The limiting points of the abscissa axis in the diagrams represent the pure compounds: 0, water; 100, α-pinene. This kind of phase diagram is typical of heteroazeotropic systems.

The lines **L$_1$** and **L$_2$** in Figs. 21a and 21b represent the compositions of the two coexisting equilibrium liquid phases as a function of temperature. The horizontal dashed lines indicate the boiling temperatures of the azeotropic mixtures, T_{az}, at a given pressure (e.g., T_{az} = 478.4 K at P = 20 atm). At any pressure, T_{az} is below the boiling point of the more volatile component (water, 486.1 K at 20 atm). The calculated boiling temperature of the α-pinene–water azeotropic mixture at 1 atm and the only experimental boiling temperature value reported for the turpentine–water mixture (367.7 K) [99] (turpentine contains 60–80% α-pinene) are in good agreement, which is evidence in favor of the thermodynamic model used here. Points 1, 2, and 3 in the horizontal lines in Figs. 21a and 21b represent the compositions of the three phases of the heteroazeotrope. The end points indicate the compositions of the two liquid phases, and the interior point represents the vapor composition.

In the liquid **L$_1$**, which is a water–α-pinene mixture, the α-pinene concentration is nearly zero (<0.001%); accordingly, the line **L$_1$** almost coincides with the ordinate axis. By contrast, the liquid **L$_2$** consists of α-pinene containing a considerable concentration of dissolved water.

In the field **L–L** in Figs. 21 and 21b, any mixture separates only into two liquid phases, whose compositions are given by the curves **L$_1$** and **L$_2$**. The field **Liq** is the field of homogeneous liquid solutions; in the fields **L–V$_1$** and **L–V$_2$**, the mixture separates only into a vapor and a liquid. In the field **Vap**, the mixture is entirely in the vapor state. The two-phase liquid–vapor equilibrium fields **L–V$_1$** and **L–V$_2$** originate

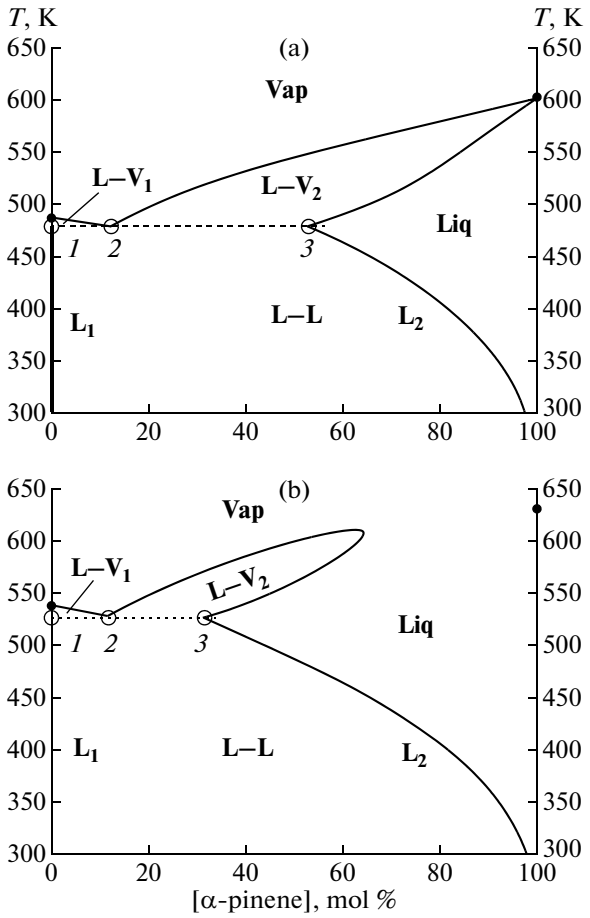

Fig. 21. *T*–*X* diagrams of the α-pinene–water system: (a) $P = 20$ atm; (b) $P = 50$ atm. Compositions of the heterozeotrope phases: (*1*, *3*) liquid phases; (*2*) vapor. For details, see main text.

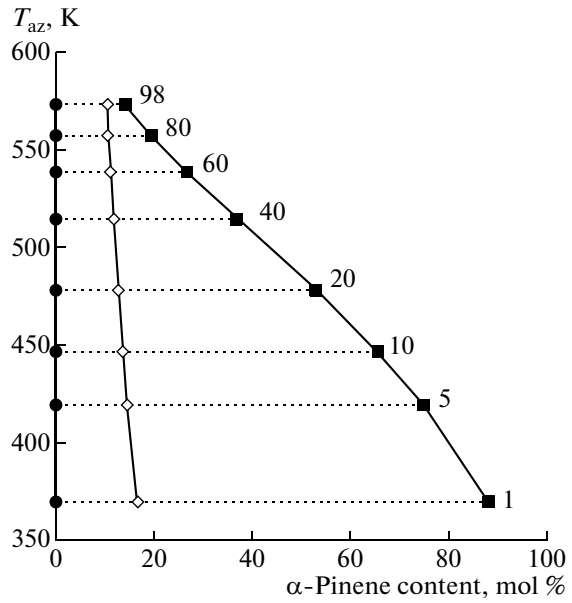

Fig. 22. Boiling temperature of azeotropic α-pinene–water mixtures as a function of their equilibrium composition. Points (from left to right) represent the compositions of the phases $\mathbf{L_1}$, **V**, and $\mathbf{L_2}$.

from the boiling point of the azeotrope. Because the boiling point of the azeotrope is very close to that of water, the field $\mathbf{L–V_1}$ is very narrow.

The curve branches bounding the field $\mathbf{L–V_2}$ are the bubble-point and dew-point branches of the binodal calculated using the model defined by Eqs. (42) and (43). Below the critical pressure of α-pinene (Fig. 21a), these branches converge at the boiling point of pure α-pinene (for example the boiling point of α-pinene at $P = 20$ atm is 602.1 K). Above the critical pressure of α-pinene (Fig. 21b), the binodal branches meet at the critical point of the mixture of the given composition.

The calculated sequence of azeotropic lines (boiling temperatures) at various pressures is shown in Fig. 22. The point indicate the compositions of the three phases—$\mathbf{L_1}$, **V**, and $\mathbf{L_2}$—corresponding to points *1*, *2*, *3* in Figs. 21a and 21b at a given pressure. As the pressure is raised at a constant temperature, the α-pinene solubility in the aqueous phase changes insignificantly (left line), in contrast with the water solubility in α-pinene (right line). As the temperature and pressure are progressively increased, the compositions and properties of the vapor and the second liquid phase come closer to each other. Above 98.3 atm, the three-phase heteroazeotropic phenomena are not observed any longer and the mixture separates into to fluid phases with nearly equal compositions.

The complete critical curve calculated via the above procedure for the α-pinene–water system is shown in Fig. 23 in the $T_{mix,cr}$–$P_{mix,cr}$ coordinates (curve *1*). The points **A** and **B** at the ends of this curve indicate the critical parameters of pure water and pure α-pinene, respectively. In going from the point **A** to the point **B** along critical curve *1* or in the opposite direction, the compositions of the binary mixture do not change. Note the anomalous shape of this curve, which has a temperature minimum. Line *2* in Fig. 23 represents, on the *T*–*P* plane, the coordinates of three-phase two-component azeotropic mixtures indicated in Fig. 22. This line ends at the minimum point of the critical curve *1*, whose coordinates are $T_{mix,cr} = 574.9$ K and $P_{mix,cr} = 98.3$ atm. The corresponding α-pinene content is 15%. As was mentioned above the azeotropic phenomena disappear as the representative point comes fairly close to the critical parameters of the mixture and the two-phase equilibrium disappears at the critical point.

α-Pinene–ethanol–water system. The α-pinene–ethanol–water system differs from the α-pinene–water system in that, in its water–ethanol and α-pinene–ethanol binary constituents, the components are unlimitedly soluble in each other, forming homo-

geneous liquid solutions. Therefore, behavior of this ternary system will depend considerably on the water/(α-pinene + ethanol) and α-pinene/ethanol ratios in the solution.

Fixing the ratio between two components in a three-component heteroazeotropic system reduces the number of degrees of freedom. As a consequence this system becomes monovariant, like a binary system, and its phase equilibria can be calculated using the procedure described above for the binary system. Calculating the phase equilibria in the ternary system examined, we fixed the ratio of the α-pinene and ethanol contents at q = α-pinene/ethanol = 1.

Figures 24a–24d display the P–T diagrams calculated for α-pinene–ethanol–water mixtures with various water contents (80, 70, 50, and 50%, respectively). Lines *1* and *1'* in these figures represent the bubble-point and dew-point branches of the binodal. The apex points of the lines are the critical points of the mixtures of the given compositions. In the field bounded by lines *1* and *1'*, the mixture separates into a vapor and a homogeneous liquid. To the right of line *1'*, the mixture is in the vapor state. The field of liquid phases is to the left of line *1*.

The discrete T_{az} and P_{az} values calculated for fixed pressures in the system are represented by open circles at the bubble-point branches of the binodals (Figs. 24a–24d, curves *1*). The upper open circle in each curve, with the coordinates (T_{end}, P_{end}), is the limiting points of azeotropy in the given mixture. Above this point (in line *1*) and up to the critical point, the mixture of the given overall composition is a homogeneous solution in equilibrium with its vapor at its boiling temperature.

Note the following specific features of the calculation of the bubble-point branch of the binodal in the case of separating three-component liquid mixture (in the case of the existence of azeotropic states). In the calculation of each point of the binodal for such systems, the initial mixture, represented as a hypothetical homogeneous liquid, is spinodally unstable; that is, StCrit < 0. This means that the chosen phase of the given composition cannot exist as a stable homogeneous liquid. This problem is solved by dividing the initial mixture into two liquid phases. Next, the equilibrium vapor composition is derived from the composition of one of the liquid phases using Eq. (46). The resulting $T_{az}(P_{az})$ or $P_{az}(T_{az})$ values define the locus of the boiling temperature of the azeotrope at the pressure P_{az}.

A comparison of the plots in Figs. 24a–24d demonstrates that, as the water content of the mixture decreases, T_{end} and P_{end} decrease and the two-phase vapor–liquid equilibrium field between lines *1* and *1'* broadens. As the proportion of the α-pinene + ethanol fraction in the mixture decreases, P_{end} and T_{end} increase. The azeotropic phenomena disappear only in mixtures containing more than 90% (α-pinene + ethanol) because water becomes completely soluble in the organic fraction.

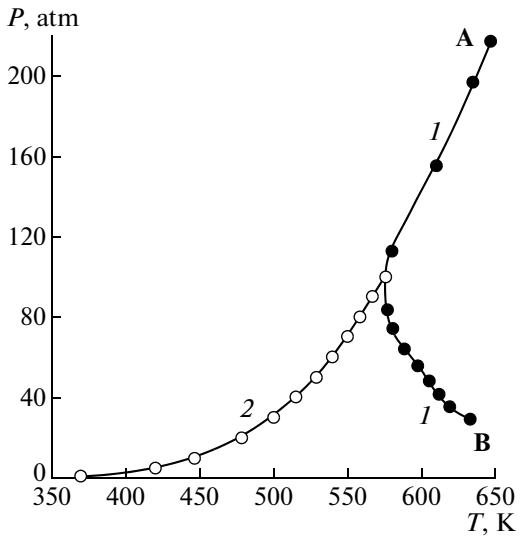

Fig. 23. (*1*) Critical curve for α-pinene–water mixtures and (*2*) the three-phase equilibrium curve in the P–T plane.

Calculation of phase equilibria to the left of the bubble-point branch of the binodal (Figs. 24a–24d, line *1*) demonstrated that this field is divided by a vertical boundary (straight line *2*, which originates from the point (T_{end}, P_{end})) into two subfields—**L**–**L** and **L**. The field **L**–**L** is the place of equilibrium between two immiscible liquid phases. In the field **L**, bounded by line *2* and by the upper branch of the binodal, the mixture is a homogenous, single-phase liquid.

These phase relations in the ternary system are valid for the case of $q = 1$ in the organic faction. In the limiting cases of $q \to \infty$ and $q \to 0$, the ternary system appears as the α-pinene–water and water–ethanol binary systems.

The compositions of the equilibrium phases at the azeotropic points at selected pressures are listed in Table 11. It follows from these data that liquid *1"* is an aqueous phase containing a minor amount of ethanol and almost no α-pinene. In the organic phase (liquid *2*), the amount of the α-pinene + ethanol fraction at low temperatures and pressures is much larger than the amount of water. The vapor phase is enriched with ethanol at low pressures and with water at higher pressures. The composition of the organic phase tends to the vapor composition as the pressure is raised.

Thus, the above approaches and computational procedures provide means to determine the phase state of binary and ternary mixtures of the α-pinene–water and α-pinene–ethanol–water types, to find the heteroazeotropic state existence conditions, and to determine the critical parameters of such mixtures in

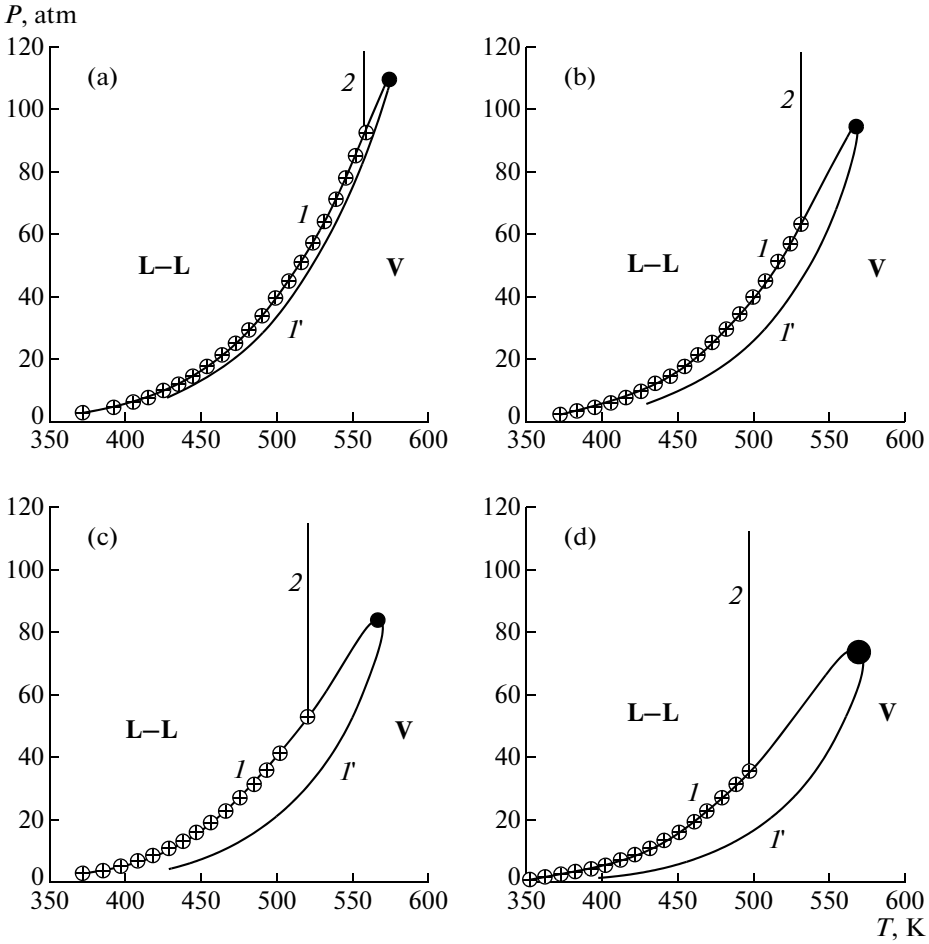

Fig. 24. *P–T* diagrams for α-pinene–ethanol–water mixtures: (a) 80, (b) 70, (c) 60, and (d) 50% water; (*1*, *1'*) bubble-point and dew-point branches of the binodal. The points at curve apices are the critical points of the mixtures; ⊕, discrete (T_{az}, P_{az}) values calculated for fixed pressures in the system.

order to optimize the reaction conditions for organic compounds in the subcritical and supercritical regions and mixture separation conditions in wide temperature, pressure, and composition ranges.

Certainly, before performing a kinetic study of any of the above reactions in the supercritical solvent, we calculated the phase state of the complex reaction mixture in order to elucidate the conditions under which this reaction takes pace. It is these calculations that enabled us to correctly choose the initial compositions of the reaction mixtures and reaction temperatures and pressures and to correctly represent the reaction routes and kinetic model equations.

CONCLUSIONS

In this work, we systematized our basic results in the field of heat-induced conversions of terpenic compounds of vegetable origin (α- and β-pinenes, turpentine, *cis*-verbenol) in supercritical fluid solvents, mainly in supercritical lower alcohols. The most important of our results is that the thermal isomerization of terpenes in supercritical media (lower alcohols) proceeds more rapidly than the same reactions in the gas or liquid phase and is equally selective toward the desired products.

The kinetic studies and thermodynamic calculations of the phase states and critical parameters of selected multicomponent multiphase terpene-containing systems enabled provided a deeper insight into the mechanism of isomerization of the terpenic compounds and into the role of the supercritical solvent in the multifold increase in the reaction rate relative to the rates observed for the same compounds in the gas or liquid phase. It was demonstrated that raising the pressure of the supercritical solvent markedly increases the rates of the reactions examined.

The chemical reactions of the above terpenes in supercritical fluid solvents can serve as a basis for advanced, high-performance technologies for obtain-

ing a wide variety of practically significant organic compounds, medicines, and fragrance substances.

REFERENCES

1. Simonsen, J., *The Terpenes*, Cambridge: Cambridge Univ. Press, 1957, vol. 2.
2. Osadchii, S.A. and Tolstikov, G.A., *Khim. Interes. Ust. Razv.*, 1997, no. 5, p. 79.
3. Il'ina, I.I., Maksimchuk, N.V., and Semikolenov, V.A., *Ross. Khim. Zh*, 2004, vol. 48, no. 3, p. 38.
4. Simakova, I.L. and Semikolenov, V.A., *Khim. Interes. Ust. Razv.*, 2003, vol. 11, no. 1, p. 271.
5. Erman, W.E., *Chemistry of the Monoterpenes: An Encyclopedic Handbook*, New York: Marcel Dekker, 1985.
6. Arbuzow, B.A., *Ber. Deut. Chem. Ges.*, 1934, vol. 67, p. 563.
7. Charlton, R.W. and Day, A.R., *Ind. Eng. Chem.*, 1937, vol. 29, p. 92.
8. Goldblatt, L.A. and Palkin, S., *J. Am. Chem. Soc.*, 1941, vol. 63, no. 12, p. 3517.
9. Nikitin, V.M., *Zh. Obshch. Khim.*, 1946, vol. 16, no. 7, p. 1041.
10. Burwell, R.L., *J. Am. Chem. Soc.*, 1951, vol. 73, no. 9, p. 4461.
11. Bochwic, B. and Kapuscinski, J., *Rocz. Chem.*, 1967, vol. 41, no. 10, p. 1767.
12. Fuguitt, R.E. and Hawkins, J.E., *J. Am. Chem. Soc.*, 1947, vol. 69, no. 2, p. 319.
13. Crowley, K.J. and Traynor, S.G., *Tetrahedron*, 1978, vol. 34, no. 18, p. 2783.
14. Gajewski, J.J. and Hawkins, C.M., *J. Am. Chem. Soc.*, 1986, vol. 108, no. 4, p. 838.
15. Garist, I.V., Petrova-Kuminskaya, S.V., Roganov, G.N., Filippenko, Z.A., and Stolyarova, L.G., *Zh. Fiz. Khim.*, 2000, vol. 74, no. 3, p. 397 [*Russ. J. Phys. Chem.* (Engl. Transl.), vol. 74, no. 3, p. 327].
16. Gajewski, J.J., Kuchuk, I., Hawkins, C., and Stine, R., *Tetrahedron*, 2002, vol. 58, no. 34, p. 6943.
17. Riistama, K. and Harva, O., *Finn. Chem. Lett.*, 1974, no. 4, p. 132.
18. Stolle, A., Brauns, C., Nuchter, M., Ondruschka, B., Bonrath, W., and Findeisen, M., *Eur. J. Org. Chem.*, 2006, no. 15, p. 3317.
19. Stolle, A., Ondruschka, B., and Bonrath, W., *Eur. J. Org. Chem.*, 2007, no. 14, p. 2310.
20. Smith, D.F., *J. Am. Chem. Soc.*, 1927, vol. 49, p. 43.
21. Conant, J.B. and Carlson, G.H., *J. Am. Chem. Soc.*, 1929, vol. 51, p. 3464.
22. Thurber, F.H. and Johnson, C.H., *J. Am. Chem. Soc.*, 1930, vol. 52, p. 786.
23. Fuguitt, R.E. and Hawkins, J.E., *J. Am. Chem. Soc.*, 1945, vol. 67, p. 242.
24. Savich, T.R. and Goldblatt, L.A., *J. Am. Chem. Soc.*, 1945, vol. 67, no. 11, p. 2027.
25. Hawkins, J.E. and Hunt, H.G., *J. Am. Chem. Soc.*, 1951, vol. 73, no. 11, p. 5379.
26. Kolicheski, M.B., Cocco, L.C., Mitchell, D.A., and Kaminski, M., *J. Anal. Appl. Pyrolysis*, 2007, vol. 80, p. 92.
27. Dorsky J., in *Perfumes: Art, Science, and Technology*, Müller, P.M. and Lamparsky, D., Eds., London: Elsevier Applied Science, 1991, p. 399.
28. Bryulyakov, Yu.E., Gorlovskii, S.I., and Shadrin, A.B., *Kompleksn. Ispol'z. Miner. Syr'ya*, 1988, no. 2, p. 21.
29. Sun, J.-H. and Zeng, T., *Linchan Huaxue Yu Gongye*, 2005, vol. 25, p. 43.
30. Summers, H.B., Hedrick, G.W., Magne, F.C., and Mayne, R.Y., *Ind. Eng. Chem.*, 1959, vol. 51, p. 549.
31. Johansson, A., *Biomass*, 1982, vol. 2, p. 103.
32. Yumrutaša, R., Alma, M.H., Özcan H., and Kaška, Ö., *Fuel*, 2008, vol. 87, p. 252.
33. Afre, R.A., Soga, T., Jimbo, T., Kumar, M., Ando, Y., Sharon, M., Somani, P.R., and Umeno, M., *Microporous Mesoporous Mater.*, 2006, vol. 96, p. 184.
34. Radbil', A.B., *Khim. Rastit. Syr'ya*, 2005, no. 1, p. 5.
35. Conceicao Cruz Costa, M., Johnstone, R.A.W., and Whittaker, D., *J. Mol. Catal. A: Chem.*, 1996, vol. 104, p. 251.
36. *Chemical Synthesis Using Supercritical Fluids*, Jessop, P.G. and Leitner, W., Eds., Weinheim: Wiley-VCH, 1999.
37. Anikeev, V.I. and Ermakova, A., *Zh. Fiz. Khim.*, 2003, vol. 77, no. 2, p. 265 [*Russ. J. Phys. Chem.* (Engl. Transl.), vol. 77, no. 2, p. 211].
38. Ikushima, Y., *Adv. Colloid Interface Sci.*, 1997, vols. 71–72, p. 259.
39. Chouchi, D., Gourgouillon, D., Courel, M., Vital, J., and Nunes da Ponte, M., *Ind. Eng. Chem. Res.*, 2001, vol. 40, p. 2551.
40. Milewska, A., Banet, OsumaA.M., Fonseca, I.M., and Numes da Ponte, M., *Green Chem.,* 2005, p. 726.
41. Bogel-Lukasik, E., Bogel-Lukasik, R., Kriaa, K., Fonseca, I., Tarasenko, Y., and Nunes da Ponte, M., *J. Supercrit. Fluids*, 2008, vol. 45, p. 225.
42. Anikeev, V.I., Ermakova, A., Chibiryaev, A.M., Kozhevnikov, I.V., and Mikenin, P.E., *Zh. Fiz. Khim.*, 2007, vol. 81, no. 5, p. 825 [*Russ. J. Phys. Chem.* (Engl. Transl.), vol. 81, no. 5, p. 711].
43. Chibiryaev, A.M., Anikeev, V.I., Ermakova, A., Mikenin, P.E., Kozhevnikov, I.V., and Sal'nikova, O.I., *Izv. Akad. Nauk, Ser. Khim.*, 2006, no. 6, p. 951.
44. Ermakova, A., Chibiryaev, A.M., Mikenin, P.E., Sal'nikova, O.I., and Anikeev, V.I., *Zh. Fiz. Khim.*, 2008, vol. 82, no. 1, p. 71 [*Russ. J. Phys. Chem.* (Engl. Transl.), vol. 82, no. 1, p. 62].
45. Yermakova, A., Chibiryaev, A.M., Kozhevnikov, I.V., and Anikeev, V.I., *J. Supercrit. Fluids*, 2008, vol. 45, p. 74.

46. Yermakova, A., Chibiryaev, A.M., Kozhevnikov, I.V., Mikenin, P.E., and Anikeev V.I., *Chem. Eng. Sci.*, 2007, vol. 62, p. 2414.

47. Chibiryaev, A.M., Ermakova, A., Kozhevnikov, I.V., Sal'nikova, O.I., and Anikeev, V.I., *Izv. Akad. Nauk, Ser. Khim.*, 2007, no. 5, p. 1188.

48. Anikeev, V.I., *Kinet. Katal.,* 2009, vol. 50, no. 2, p. 300 [*Kinet. Catal.* (Engl. Transl.), vol. 50, no. 2, p. 284].

49. Tkachev, A.V., *Issledovanie letuchikh veshchestv rastenii* (Volatile Compounds of Plants), Novosibirsk: Ofset, 2008.

50. Marquard, D.W., *J. Soc. Ind. Appl. Math.*, 1963, vol. 11, p. 431.

51. Valko, P. and Vajda, S., *Muszaki feladatok megoldasa szemelyi szamitogepekkel*, Budapest: Muszaki Konyvkiado, 1987.

52. Vajda, S., Valko, P., and Turanyi, T., *Int. J. Chem. Kinet.*, 1985, vol. 17, p. 55.

53. Vajda, S., Valko, P., and Yermakova, A., *Comput. Chem. Eng.,* 1986, vol. 10, no. 1, p. 49.

54. Franck, E.U. and Weingartner, H., in *Chemical Thermodynamics,* A Chemistry for the 21st Century Monograph, London: Blackwell Science, 1999, ch. 9, p. 348.

55. Marshall, W.L. and Franck, E.U., *J. Phys. Chem. Ref. Data*, 1981, vol. 10, no. 2, p. 296.

56. Anikeev, V.I., Menion, D., and Ermakova, A., *Zh. Fiz. Khim.*, 2001, vol. 75, no. 8, p. 1387 [*Russ. J. Phys. Chem.* (Engl. Transl.), vol. 75, no. 8, p. 1259].

57. Anikeev, V.I., Yermakova, A., Semikolenov, V.A., and Goto, M., *J. Supercrit. Fluids*, 2005, vol. 33, p. 243.

58. Klein, S.A. and Harwey, A.H., *NIST/ASME Steam Properties: Formulation for General and Scientific Use*, NIST Standard Reference Database, Version 2.01, Gaithersburg, Md.: NIST, 1997.

59. Vajda, S., Valko, P., and Yermakova, A., *Comput. Chem. Eng.*, 1986, vol. 10, no. 1, p. 49.

60. Ermakova, A., Bibin, V.N., Brin, E.F., Valko, P., and Vaida, S., *Kinet. Katal.,* 1985, vol. 26, no. 3, p. 711.

61. Hunt, H.G. and Hawkins, J.E., *J. Am. Chem. Soc.*, 1950, vol. 72, no. 12, p. 5618.

62. Hawkins, J.E. and Vogh, J.W., *J. Phys. Chem.*, 1953, vol. 57, no. 9, p. 902.

63. Sasaki, T., Eguchi, S., and Ishii, T., *J. Org. Chem.*, 1969, vol. 34, no. 12, p. 3749.

64. Johanson, A.J., McKennon, F.L., and Goldblatt, L.A., *Ind. Eng. Chem.*, 1948, vol. 40, no. 3, p. 500.

65. Banthorpe, D.V. and Whittaker, D., *Chem. Rev.,* 1966, vol. 66, no. 6, p. 643.

66. Rocha, W.R., Milagre, H.M.S., and de Almeida, W.B., *J. Mol. Struct.*, 2001, vol. 544, p. 213.

67. Joback, K.G. and Reid, R.C., *Chem. Eng. Commun.,* 1987, vol. 57, p. 233.

68. Pines, H. and Ryer, J., *J. Am. Chem. Soc.*, 1955, vol. 77, p. 4370.

69. Cocker, W., Hanna, D.P., and Shannon, P.V.R., *J. Chem. Soc. C*, 1968, vol. 5, p. 489.

70. Shimazu, K., Hattori, H., and Tanabe, K., *J. Catal.,* 1977, vol. 48, p. 302.

71. Lesage, P., Candy, J.-P., Hirigoyen, C., Humblot, F., Leconte, M., and Basset, J.-M., *J. Mol. Catal. A: Chem.*, 1996, vol. 112, p. 303.

72. Meyer, U. and Hoelderich, W.F., *J. Mol. Catal. A: Chem.,* 1999, vol. 142, p. 213.

73. Carey, F. and Sundberg, R., *Advanced Organic Chemistry*, part A: *Structure and Mechanisms*, New York: Kluwer/Plenum, 2000, 4th ed., p. 836.

74. Maksimchuk, N., Simakova, I., and Semikolenov, V., *React. Kinet. Catal. Lett.*, 2004, vol. 82, no. 1, p. 165.

75. Ringer, K.L., Davis, E.M., and Croteau, R., *Plant Physiol.,* 2005, vol. 137, p. 863.

76. Baliga, B.T. and Whalley, E., *Can. J. Chem.*, 1965, vol. 9, p. 2453.

77. Narayan, R. and Antal, M.J., *J. Am. Chem. Soc.*, 1990, vol. 112, p. 1927.

78. Akiya, N. and Savage, P.E., *J. Phys. Chem. A*, 2000, vol. 104, p. 4441.

79. Roberts, C.B., Zhang, J., Chateauneuf, J.E., and Brennecke, J.F., *J. Am. Chem. Soc.*, 1995, vol. 117, p. 6553.

80. Klein, M., Mentha, Y.G., and Torry, L.A., *Ind. Eng. Chem. Res.*, 1992, vol. 31, p. 182.

81. Zhou, L., Erkey, C., and Akgerman, A., *AIChE J.,* 1995, vol. 41, p. 2122.

82. Meyer, J.C., Marrone, P.A., and Tester, J.W., *AIChE J.,* 1995, vol. 41, p. 2108.

83. Guo, Y. and Akgerman, A., *Ind. Eng. Chem. Res.*, 1997, vol. 36, p. 4581.

84. Tomita, K., Koda, S., and Oshima, Y., *Ind. Eng. Chem. Res.*, 2002, vol. 41, p. 3341.

85. Ellington, J.B., Park, K.M., and Brennecke, J.F., *Ind. Eng. Chem. Res.*, 1994, vol. 33, p. 956.

86. Roek, D.P., Chateauneuf, J.E., and Brennecke, J.F., *Ind. Eng. Chem. Res.*, 2000, vol. 39, p. 3090.

87. Yu, J. and Eser, S., *Ind. Eng. Chem. Res.*, 1997, vol. 36, p. 585.

88. Collins, N.A., Debenedetti, P.G., and Sundaresan, S., *AIChE J.,* 1988, vol. 34, p. 1211.

89. Kajimoto, O., *Chem. Rev.,* 1999, vol. 99, p. 355.

90. Anikeev, V.I., Ermakova, A., Golovizin, A.V., and Goto, M., *Zh. Fiz. Khim.*, 2004, vol. 78, no. 10, p. 1769

[*Russ. J. Phys. Chem.* (Engl. Transl.), vol. 78, no. 10, p. 1553].

91. Sandler, S.I., *Chemical, Biochemical, and Engineering Thermodynamics*, New York: Willey, 2006, 4th ed., p. 960.
92. Anikeev, V.I. and Ermakova, A., *Teor. Osn. Khim. Tekhnol.*, 1998, vol. 32, no. 5, p. 508 [*Theor. Found. Chem. Eng.* (Engl. Transl.), vol. 32, no. 5, p. 462].
93. Peng, D.Y. and Robinson, D.B., *AIChE J.,* 1977, vol. 23, no. 2, p. 137.
94. Krichevskii, I.R., *Fazovye ravnovesiya v rastvorakh pri vysokikh davleniyakh* (Phase Equilibria in Solutions at High Temperatures), Moscow: Goskhimizdat, 1952, p. 196.
95. Ermakova, A. and Anikeev, V.I., *Teor. Osn. Khim. Tekhnol.*, 2000, vol. 34, no. 1, p. 57 [*Theor. Found. Chem. Eng.* (Engl. Transl.), vol. 34, no. 1, p. 51].
96. Ermakova, A., Anikeev, V.I., and Sazhina, O.V., *Teor. Osn. Khim. Tekhnol.*, 2005, vol. 39, no. 1, p. 88 [*Theor. Found. Chem. Eng.* (Engl. Transl.), vol. 39, no. 1, p. 85].
97. *Termodinamika ravnovesiya zhidkost'-par* (Liquid–Vapor Equilibrium Thermodynamics), Morachevskii, A.G., Ed., Leningrad: Khimiya, 1980, p. 168.
98. Michelsen, M.L., *Fluid Phase Equilib.*, 1982, vol. 9, p. 21.
99. Glukhareva, M.I., Drozdov, N.P., Ermakova, L.A., et al., *Spravochnik lesokhimika* (Wood Chemist's Handbook), Moscow: Lesnaya Prom-st., 1974, p. 376.